[AMERICAN JOURNAL OF SCIENCE, VOL. 264, JUNE 1966, P. 428-480]

EXPERIMENTAL DATA FOR THE SYSTEM MgO-FeO-Fe_2O_3-$CaAl_2Si_2O_8$-SiO_2 AND THEIR PETROLOGIC IMPLICATIONS*

P. L. ROEDER** and E. F. OSBORN

The Pennsylvania State University, University Park, Pennsylvania

ABSTRACT. Liquidus data are presented for the system MgO-FeO-Fe_2O_3-$CaAl_2Si_2O_8$-SiO_2, determined at one atm total pressure and at oxygen partial pressures ranging from 10^{-11} to $10^{-0.7}$ atm. Equilibrium relations among olivine, pyroxene, anorthite, magnetite, tridymite, liquid, and a gas phase have been determined for the four levels of oxygen partial pressure: $10^{-0.7}$, 10^{-7}, 10^{-9}, 10^{-11} atm. Magnetite and pyroxene are compatible phases at the first three but not at the last. Therefore at oxygen partial pressures as low as 10^{-9} atm, anorthite, pyroxene, magnetite, and tridymite coexist with liquid. This liquid is the end result of fractional crystallization of basalt-like liquids in the system at oxygen partial pressures of 10^{-9} atm or higher. Composition[1] and temperature data for this residual liquid at three oxygen partial pressures are as follows:

$pO_2 = 10^{-0.7}$ atm, 1185°C, 57 SiO_2, 8 iron oxide, 9 MgO, 9 CaO, 17 Al_2O_3
$pO_2 = 10^{-7}$ atm, 1155°C, 55 SiO_2, 14 iron oxide, 6 MgO, 9 CaO, 16 Al_2O_3
$pO_2 = 10^{-9}$ atm, 1120°C, 51 SiO_2, 21 iron oxide, 6 MgO, 8 CaO, 14 Al_2O_3

The part of the system in which anorthite is one of the crystalline phases present is depicted as a tetrahedron—the anorthite-saturation tetrahedron. This permits visual representation in a single diagram of the phase relations of most interest in geologic applications. The anorthite-saturation tetrahedron is compared with the tetrahedral diagram for the quaternary system MgO-FeO-Fe_2O_3-SiO_2 to estimate the effect on phase relations of adding CaO and Al_2O_3 to the quaternary system, or in other words the effect of the presence of anorthite on phase relations among olivine, pyroxene, magnetite, tridymite, liquid, and gas. The general nature of courses of crystallization is not changed by the addition of anorthite. Liquid compositions, temperatures, and oxygen partial pressures however are much closer to those of basalts and andesites with anorthite present. With fractional crystallization at an oxygen partial pressure of 10^{-7} atm, the residual liquid has an andesitic composition as indicated above. On the other hand, the course of fractional crystallization of liquids in the system at constant total bulk composition (constant oxygen content, as in a closed system) is toward low oxygen partial pressures and ferrogabbroic liquids. The residual liquid in this latter instance approaches the composition, 45 SiO_2, 38 iron oxide, 6 CaO, and 11 Al_2O_3, where it is in equilibrium with anorthite, fayalite, magnetite, and tridymite at 1050°C and an oxygen partial pressure of about 10^{-11} atm.

Liquid variation curves are drawn for the system showing the change in composition of the liquid in equilibrium with anorthite, magnetite, tridymite, and either pyroxene or olivine, as a function of oxygen partial pressure. From these curves it is evident that fractional crystallization of a simplified basaltic magma in the system may produce a residual liquid ranging in SiO_2 content from 45 to 57 and in iron oxide content from 38 to 8 weight percent as the oxygen partial pressure of the residual liquid varies from 10^{-11} to $10^{-0.7}$ atm. A higher SiO_2 content of the residual liquid at any oxygen partial pressure will undoubtedly result if Na_2O is present and plagioclase crystallizes rather than anorthite, permitting the plagioclase continuous reaction series to have its effect on liquid compositions.

* Contribution No. 64-63, College of Mineral Industries, The Pennsylvania State University, University Park, Pennsylvania. A part of the data appearing herein is included in the Ph.D. thesis of P. L. Roeder, "Phase Relations in the Mg_2SiO_4-$CaAl_2Si_2O_8$-FeO-Fe_2O_3-SiO_2 System and their Bearing on Crystallization of Basaltic Magma", The Pennsylvania State University, University Park, Pennsylvania, 1960.

**Present address: Queen's University, Kingston, Ontario, Canada.

[1] In weight percent, with all iron oxide calculated as Fe_3O_4.

INTRODUCTION

If basaltic magma is crystallized under equilibrium conditions and as a closed system, a body will result consisting essentially of pyroxene, plagioclase, and magnetite. Each of these minerals will be uniform in composition throughout the body, that is, each crystal will be homogeneous, and all will be identical in composition, but the ratio of the masses of the several crystals may differ from place to place. If on the other hand this magma is fractionally crystallized, other phases in addition to pyroxene, plagioclase, and magnetite may be present in the end product (for example, olivine), crystals may not be homogeneous, and different crystals of the same phase may not have identical compositions. Various fractions of the crystallized body may differ consequently in respect to composition of the constituent phases and in number, types, and proportions of the phases present. It is the behavior during fractional crystallization that is of especial interest to geologists, for by this process a diversity of rock types can be produced from a single primary magma. Phase relations during fractional crystallization can be estimated if equilibrium relations are known. Indeed, the behavior of a system in crystallizing with *perfect* fractionation is completely determined, and if the equilibrium relations are known is predictable from them. While equilibrium relations are not known for a system of the composition of basalt, those for the simpler system, MgO-FeO-Fe_2O_3-SiO_2, have been obtained and may be usefully applied to the more complex basalt systems (Osborn, 1959).

From an analysis of data for the system MgO-FeO-Fe_2O_3-SiO_2 there is the suggestion that the manner of change of oxygen partial pressure during fractional crystallization of a basalt may be a very important factor affecting especially the distribution of iron oxide and silica in the fractions (Osborn, 1959). In the system MgO-FeO-Fe_2O_3-SiO_2, if mixtures of the nature of a simplified basalt (those which will crystallize under equilibrium conditions to pyroxene plus magnetite) are fractionally crystallized as a system closed to oxygen, the residual liquid becomes rich in iron oxide. If, however, the oxygen partial pressure is maintained approximately constant or increases during the fractional crystallization of such mixtures (necessitating an increase in oxygen content of the mass), the liquid composition does not move to such high iron oxide compositions but instead may move to moderately high silica compositions. In general for this latter case, the higher the partial pressure of oxygen during the later stages of crystallization, the higher will be the silica content and the lower the iron oxide content of the residual liquid.

If we add CaO to these four components, a closer approach to basalt compositions is achieved. An estimate of phase relations can be made from existing data (Osborn, 1962). With CaO added some changes in phase assemblages occur, as for example, a diopsidic pyroxene is stable as well as a pigeonitic pyroxene, but the general nature of crystallization

of mixtures of simplified basalt composition as far as distribution of iron oxide among the liquid and crystalline fractions is concerned seems not to be changed because of the CaO additions.

In the experimental work discussed in this paper, Al_2O_3 and CaO were both added to the MgO-FeO-Fe_2O_3-SiO_2 system. They were added as $CaAl_2Si_2O_8$ and thus in a fixed 1:1 mole ratio. The resulting system, MgO-FeO-Fe_2O_3-$CaAl_2Si_2O_8$-SiO_2, was studied in the compositional region of principal geologic interest to determine liquidus relations over a wide range of oxygen partial pressures, at a total pressure of one atm. Simplified basalts and andesites in this system approach much more closely their natural analogues than in the systems studied previously, for the feldspar anorthite is present as a phase as well as the ferromagnesian minerals and silica, and liquidus temperatures and oxygen partial pressures approach closely those of basalts (Fudali, Muan, and Osborn, 1961). In determining phase relations for this system a further step is thus being made toward understanding the phase relations for basalt and related magmas.

In presenting data for the system MgO-FeO-Fe_2O_3-$CaAl_2Si_2O_8$-SiO_2 certain approximations and simplifying devices will be used in order to develop diagrams that show phase relations for this complex system in a relatively uncomplicated manner. A first approximation is to treat the system as quinary, neglecting the fact that CaO and Al_2O_3 are not always present in a phase in precisely a 1:1 mole ratio. Fortunately, making this approximation for purposes of plotting the data and portraying phase relations does not introduce any error that is significant in the arguments or conclusions of this paper. Throughout the paper the system will therefore simply be referred to as quinary.

GENERAL CONSIDERATIONS AND METHOD OF PRESENTATION OF DATA

In his treatment of the FeO-Fe_2O_3-SiO_2 system Muan (1955) made the important distinction between crystallization at constant pO_2[2] and crystallization at constant total composition. In the former, the oxygen content of the condensed phases changes during crystallization, in the latter the oxygen content of the condensed phases remains constant. Ordinarily for silicate systems this latter case only is considered, but where iron oxide is a component pO_2 becomes an important variable, and one case which can be treated quantitatively and illustrated with reasonable clarity even in very complex systems is that of constant pO_2. In describing crystallization paths for mixtures in the FeO-Fe_2O_3-SiO_2 system, Muan (1955) called attention to the fact that during crystallization at constant pO_2 the liquid composition changes along an oxygen isobar on the liquidus surface, while the total composition of the mixture changes along an iso-silica line. Consequently, the composition of the

[2] Throughout this paper the term pO_2 signifies oxygen partial pressure. Wherever the term "isobaric" is used it refers to constant pO_2. All experimental work was carried out at a total gas pressure of one atm.

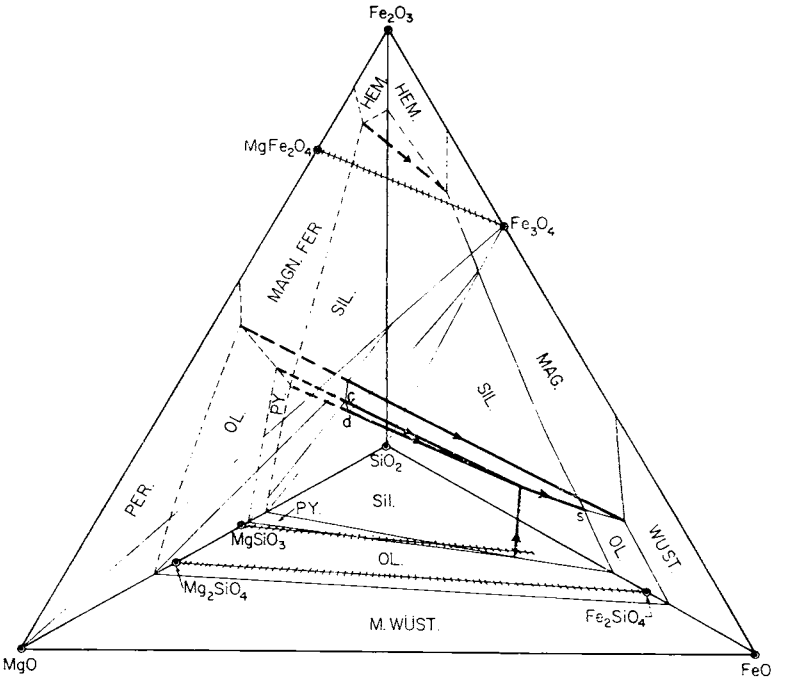

Fig. 1. Tetrahedron to illustrate liquidus phase relations in the quaternary system MgO-FeO-Fe_2O_3-SiO_2 in air (after Muan and Osborn, 1956). Univariant boundary curves on three of the bounding ternary systems are shown by light lines. The heavy lines represent univariant curves within the tetrahedron along which three crystalline phases, one liquid, and vapor are in equilibrium. Arrows indicate the direction of decreasing temperature. Lines are solid if experimentally determined, dashed if inferred. Composition joins for three solid solution series are shown by cross-hatched lines. The triangular plane MgO-Fe_3O_4-SiO_2 passing through the tetrahedron is shown by light lines and is presented separately in figure 2. Abbreviations used are: HEM = hematite, MAGN. FER = magnesioferrite, SIL = silica, MAG = magnetite, PER = periclase, OL = olivine, PY = pyroxene, WÜST = wüstite, M. WÜST = magnesiowüstite.

liquid at any stage in the crystallization is a function of the manner and degree of change of pO_2 as well as the other variables.

Addition of MgO to the FeO-Fe_2O_3-SiO_2 system requires use of a tetrahedron to represent the composition of the phases. In figure 1 the heavy solid lines are quaternary univariant lines representing liquid compositions in equilibrium with three crystalline phases and a vapor. The range in composition of the crystalline phases is indicated, and by the use of tie lines the composition of a crystalline phase in equilibrium with a liquid on the univariant line can be shown (Muan and Osborn, 1956). The pO_2 of the vapor phase in equilibrium with the liquid is more difficult to show. Whereas in the triangular diagram representing phase relations for the system FeO-Fe_2O_3-SiO_2 the pO_2 of liquids at liquidus temperatures could be shown by isobaric lines drawn on the

liquidus surface (Muan, 1955), isobaric surfaces[3] within a tetrahedron are required to represent analogous data. Thus for the tetrahedron of figure 1 liquid compositions at liquidus temperatures for a given pO_2 can be shown by an irregular surface of constant pO_2 passing through the tetrahedron from the FeO-Fe_2O_3-SiO_2 face to the MgO-SiO_2 edge. A series of such isobaric surfaces within the tetrahedron would indicate pO_2-liquid composition relations. We have not drawn such surfaces because a confusion of lines would result. Instead, for showing the composition of liquid at constant pO_2 the device is used of recalculating points on an isobaric surface so that they lie on a triangular plane within the tetrahedron, for example, the MgO-Fe_3O_4-SiO_2 plane, and then sketching this plane as a separate triangular diagram. Divariant phase boundaries and univariant lines intersected by an isobaric surface are shown on the isobaric plane as univariant lines and invariant points respectively. The isobaric plane, MgO-Fe_3O_4-SiO_2, for a given pO_2 is derived from an isobaric surface of this pO_2 simply by recalculating all iron oxide as Fe_3O_4 and is equivalent to projecting points on the isobaric surface to the MgO-Fe_3O_4-SiO_2 plane along lines extending from the oxygen apex of the MgO-SiO_2-Fe-O system. The air isobaric surface, representing liquidus phase relations in air atmosphere (constant pO_2 of $10^{-0.7}$ atm) is thus represented by the isobaric plane shown by the light lines in figure 1 and also as the equilateral triangle in figure 2, after Muan and Osborn (1956). The actual deviation of the Fe_2O_3/FeO ratio of the isobaric surface from that of the isobaric plane can be shown by a series of Fe_2O_3/FeO contours. These contours, shown by triple-dot-dash lines on the air isobaric plane of figure 2, indicate the actual composition of the liquid as determined by analysis.

This isobaric *plane* for the MgO-FeO-Fe_2O_3-SiO_2 system (fig. 2) can be used for describing courses of crystallization at the constant pO_2 of $10^{-0.7}$ atm just as an isobaric *line* is used for the FeO-Fe_2O_3-SiO_2 system. During crystallization of a mixture in the MgO-FeO-Fe_2O_3-SiO_2 system at this constant pO_2 of $10^{-0.7}$ atm, the liquid as it changes composition must stay on the surface represented by this plane (fig. 2). The composition change of the liquid can therefore be followed precisely. The point *c* represents a peritectic and *d* a eutectic under this isobaric condition. Compositions of crystalline phases can be recalculated or projected onto the isobaric plane by the same method used for the liquid phase and are shown as cross-hatched lines in figure 2. As described by Presnall (ms), an isobaric plane such as figure 2 can be used in the same way as the usual phase equilibrium diagram of a condensed ternary system for illustrating the phase relations.

In the present study CaO and Al_2O_3 have been added as $CaAl_2Si_2O_8$ to part of the MgO-FeO-Fe_2O_3-SiO_2 system. Inasmuch as compositions

[3] Hereafter the term "isobaric surface" will be used for the irregular surface within the tetrahedron which represents the actual liquidus at the particular pO_2 under consideration. The term "isobaric plane" will be used for the equilateral triangle which is derived from the isobaric surface by recalculation of liquid compositions or by projection.

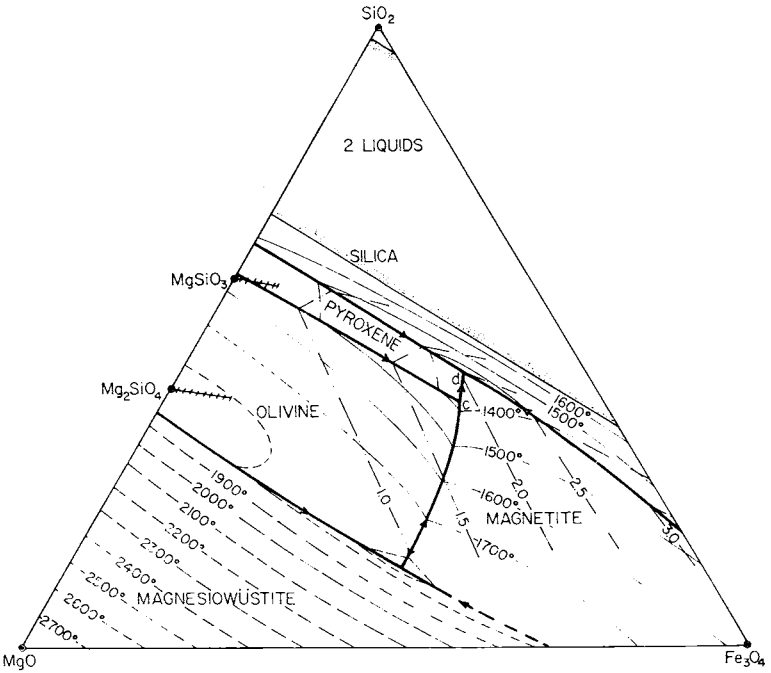

Fig. 2. Diagram to illustrate liquidus phase relations in the system MgO-FeO-Fe_2O_3-SiO_2 at $pO_2 = 10^{-0.7}$ atm (air). The position of this isobaric plane[3] within the tetrahedron is shown in figure 1. The heavy lines represent isobaric[2] univariant boundary curves, and the light solid and dashed lines are isotherms on the liquidus surface. The light dashed-triple dot lines are curves of constant Fe_2O_3/FeO ratio in the liquid and indicate the position of the air isobaric surface within the tetrahedron of figure 1. Compositions of olivine and pyroxene solid solutions in the system have been recalculated with all iron oxide as Fe_3O_4 so that their composition joins, shown as cross-hatched lines, lie in this plane (after Muan and Osborn, 1956).

richer in MgO than Mg_2SiO_4 are of little or no petrologic interest, and in order to simplify the representation of this very complex system wherever possible, Mg_2SiO_4 will be used as a component instead of MgO in much of the subsequent discussion. The resulting five component system is Mg_2SiO_4-FeO-Fe_2O_3-$CaAl_2Si_2O_8$-SiO_2.

The representation of equilibrium phase relations in a five component system is fraught with difficulties. For a ternary system we may use a triangle whose apices are the three components and whose sidelines are the three limiting binary systems. For a quaternary system, a tetrahedron may be used, having the four components as apices and the four faces as the four limiting ternary systems. In this latter case three dimensions are required for the model, but useful sketches in perspective in two dimensions can be made. In the case of a quinary system there are five limiting systems which are themselves quaternary systems. These limiting quaternary systems can be sketched, but there is no way of showing the complete phase relations for the quinary system in a single

model or diagram. With certain simplifications, however, a quinary system can be sketched in a way that will give a reasonably clear and meaningful picture of significant relations.

One very useful approach both in its investigation and in its portrayal is to fix the system at a series of constant pO_2's. By doing this the complexity is reduced by one variable or by one dimension. This technique has been discussed above for the quaternary system MgO-FeO-Fe_2O_3-SiO_2 where a tetrahedron (fig. 1) is required to illustrate phase relations in a single diagram, but with the pO_2 held constant at $10^{-0.7}$ atm, phase relations at this pO_2 can be shown by using a triangular plane (fig. 2). A series of such isobaric triangles can be drawn from data obtained at different pO_2's as done by Muan and Osborn (1956), and this series then can give a quantitative picture of phase relations within the tetrahedron. Similarly, a series of isobaric tetrahedra is one of the possible ways of studying and presenting the data for the quinary system, and this is the principal method used in this paper. Such an isobaric tetrahedron, without however showing internal phase boundaries

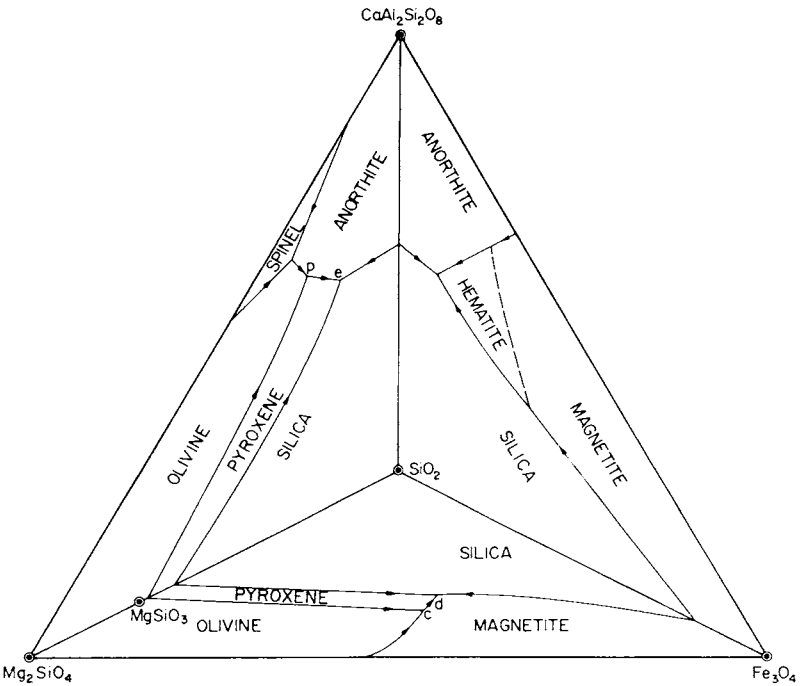

Fig. 3. Tetrahedron to illustrate manner of presentation of phase relations at a constant pO_2, in this case for air ($10^{-0.7}$ atm), for the five-component system Mg_2SiO_4-FeO-Fe_2O_3-$CaAl_2Si_2O_8$-SiO_2. Boundary curves are shown on three of the four bounding faces of the isobaric tetrahedron. The left face is after Andersen (1915), the base is part of the plane shown in figure 2 after Muan and Osborn (1956), and the right face which was studied in the present work is shown separately in figure 7. Liquidus phase relations within the tetrahedron have been omitted.

or those on the front face, is sketched in figure 3. The three faces of the tetrahedron having Fe_3O_4 as an apex are air-isobaric planes in quaternary systems, for example, the right face is the air isobaric plane in the tetrahedron for the system $CaAl_2Si_2O_8$-FeO-Fe_2O_3-SiO_2. The left face of figure 3 is the diagram for the condensed system Mg_2SiO_4-$CaAl_2Si_2O_8$-SiO_2 after Andersen (1915). This tetrahedron (fig. 3) in its relation to the quinary system is analogous to the triangle of figure 2 in its relations to the quaternary system of figure 1. In an isobaric tetrahedron such as figure 3, the recalculated compositions of liquids and crystals can be represented for the given condition of constant pO_2. For this tetrahedron, just as for the isobaric plane of figure 2, all iron oxide is recalculated as Fe_3O_4. Divergence of actual liquid compositions from this 1:1 Fe_2O_3/FeO ratio might be shown on the faces of the tetrahedron by lines of constant Fe_2O_3/FeO ratio, as done in figure 2, and within the tetrahedron by surfaces of constant Fe_2O_3/FeO ratio.

METHODS OF INVESTIGATION

The quenching technique first described by Day, Shepherd, and Wright (1906) was used in this study. A charge of material weighing approximately 0.1 gram was placed in a platinum or palladium-silver envelope which in turn was inserted into a vertical-tube resistance furnace. The top of the envelope was left open to facilitate attainment of equilibrium between the gas phase and the charge.

The time necessary to achieve equilibrium for mixtures in this study is highly variable, depending upon the temperature, the chemical composition of the mixture, the amount of liquid present, and the pO_2. Approximately four hundred experimental runs are listed in the data tables (app., p. 462-480), although more than seven hundred runs were made in the course of this study. Many of these runs were made in order to determine the length of time needed to achieve a close approach to equilibrium for different compositions and experimental conditions. In such test runs, temperature and pO_2 were approached from both higher and lower levels as one means of estimating whether or not time was sufficient for attainment of equilibrium among the phases. As a result of these tests we feel certain that the data presented represent substantially equilibrium relations.

The atmosphere within the furnace was controlled by mixing CO_2 and H_2 in the appropriate proportions to give the desired pO_2 at the temperature of the run. The CO_2:H_2 ratio needed to give a desired pO_2 can be calculated by knowing the equilibrium constants for the following equations as a function of temperature (Muan, 1958).

$$CO_2 + H_2 = CO + H_2O$$
$$2CO_2 = 2CO + O_2$$

The gas mixer used in the present study to mix CO_2 and H_2 is similar to that described by Darken and Gurry (1945). The capillary flow meters were calibrated using a standard wet-test meter and checked by runs made in the Fe-O system (Muan, 1958). The total flow rate

through the furnace was maintained at a value corresponding to a linear flow rate of approximately 1 centimeter per second (Darken and Gurry, 1945).

The temperature of the runs was measured by means of a Pt versus 90Pt-10Rh thermocouple standardized at periodic intervals using as fixed points certain melting points defined as follows: gold 1063°C, diopside ($CaMgSi_2O_6$) 1391.5°C, and pseudowollastonite ($CaSiO_3$) 1544°C. Because of the danger of contamination of the thermocouple, most runs were made without the thermocouple in the furnace, and so the temperature measurements were made before and after each run.

Mixtures used in this study were prepared from chemically analyzed reagents. The reagents were heat treated as follows: MgO at 1400° for 24 hours, SiO_2 at 400° for 24 hours, then at 1200° for 24 hours, Fe_2O_3 at 400° for 12 hours, $CaCO_3$ at 300° for 24 hours, Al_2O_3 at 1200° for 24 hours. The reagents were weighed to give a ten-gram sample of the desired final composition and were then ground under ethyl alcohol to approximately 200 mesh. The mixtures were fired to a temperature above the liquidus in a globar resistance furnace for 12 hours or in a gas-air combustion furnace for approximately one hour. The mixtures were then quenched and crushed to pass an 80 mesh screen and were used for the experimental runs in the phase equilibrium studies. Except for very iron-rich mixtures, all samples quenched to a glass.

Iron in the sample alloys to some extent with the platinum envelope containing it, changing the total composition of the sample. Analysis showed that in air ($pO_2 = 10^{-0.7}$ atm) there is negligible loss of iron to the platinum, but at a pO_2 of 10^{-9} and 10^{-11} the iron loss is considerable. All samples which were run at a low pO_2 in platinum were analyzed for total iron, and the sample compositions were then recalculated to 100 percent. In order to circumvent this problem containers made of a palladium-silver alloy (Muan, 1961) were used in many runs at 10^{-7}, 10^{-9}, and 10^{-11} atm. A 40 percent Pd-60 percent Ag alloy was used for all the runs in palladium-silver shown in tables 4, 5, and 6. The runs analyzed by C. O. Ingamells (shown in table 10) were run at a later time, and only the 45 percent Pd-55 percent Ag alloy was available. As seen in table 10 the later runs at 10^{-11} atm did lose some iron to the container.

Some samples were analyzed for their ferrous iron content in order to determine the change in ferrous to ferric ratio in the charge as a function of temperature, composition, and pO_2. The results are shown in table 10.

Samples were analyzed for divalent iron by the potassium permanganate method as described by Hillebrand and others (1953). Total iron was determined by reducing with stannous chloride, using sodium diphenylamine indicator, and titrating with standardized potassium dichromate solution.

Except for silica and anorthite the crystalline phases in this study exhibit significant variation in composition. The methods used in attempting to determine this variation in composition are discussed below.

The amount of Fe^{+2} substituting for Mg^{+2} in the olivine structure was found independently by two methods. One method involved the measurement of refractive indices which were then plotted on a curve determined by Bowen and Schairer (1935). In the other method samples were X-rayed and the shift in "d" spacing of the (130) reflection was measured using an internal standard of annealed NaCl, and this value was plotted on the curve of "d" spacing versus composition as given by Yoder and Sahama (1957). The effect of calcium substitution was neglected.

Determination of the composition of the pyroxene in equilibrium with liquid presented a problem. It was not possible to determine the polymorphic form of the pyroxene which was present at the temperature of the runs. X-ray diffraction lines of the quenched samples closely resembled the lines of clinopyroxene; however, it was impossible to index completely the diffraction patterns. Because of the small size of the crystals, the possibility of more than one structural modification or of disordered structure (Brown and Smith, 1963), and the lack of suitable data correlating composition with physical properties, no reliable compositional or structural data on the pyroxenes were obtained.

The amount of Al_2O_3 in solid solution in hexagonal Fe_2O_3 was found by measuring the shift in "d" spacing of the (124) reflection and then plotting this value on a curve published by Muan and Gee (1956).

The composition of the spinel phase in equilibrium with other crystalline phases and liquid shows a large variation. In the system under study spinel can be represented by six end members: $FeFe_2O_4$, $FeAl_2O_4$, $MgFe_2O_4$, $MgAl_2O_4$, Al_2O_3, and Fe_2O_3. The spinel modifications of Fe_2O_3 and Al_2O_3 are cation-deficient spinels. Inasmuch as the results of Atlas and Sumida (1958) and the present work indicate that cation deficiency has only a small effect on the cell dimensions of spinel, the variation in the cation to anion ratio will be neglected and only the first four end numbers listed above will be considered. Because of the relatively small temperature range over which the present work was conducted, the change in unit-cell size with the temperature of quenching as described by Paladino (1960) will be neglected. When Mg^{+2} substitutes for Fe^{+2} in $FeFe_2O_4$ there is little change in the "d" spacing of the (311) reflection. This reflection was used because it gave the most intense X-ray peak and could be found even when the amount of spinel present was small. The (311) "d" spacing of $FeFe_2O_4$ was found to be 2.531 (compared to 2.531 from Atlas and Sumida) at 1200° while that of $MgFe_2O_4$ was 2.530 (compared to 2.531 from Paladino). The change in the (311) "d" spacing in the $MgAl_2O_4$-$FeAl_2O_4$ series is greater than that in the $MgFe_2O_4$-$FeFe_2O_4$ series but is small compared to the effect of Al^{+3} substitution for Fe^{+3}. Thus the (311) "d" spacing can be used as a rough guide to indicate Al_2O_3 content. Figure 4 is a plot of the (311) "d" spacing against mole percent Al_2O_3 in the spinel. Of the four series

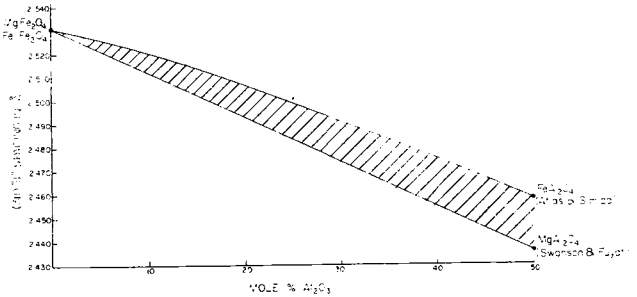

Fig. 4. Curves illustrating the change in (311) "d" spacing of spinel as a function of mole percent Al_2O_3. Although only two curves are shown, this diagram represents four binary solid solution series as explained in text. The area between the two curves, indicated by diagonal lines, is assumed to encompass all spinel solid solutions having as end members: Fe_3O_4, $MgFe_2O_4$, $FeAl_2O_4$, $MgAl_2O_4$. A particular "d" spacing plotted on this diagram would indicate a spinel with an Al_2O_3 content within a certain range.

which are represented ($MgFe_2O_4$-$FeAl_2O_4$, $MgFe_2O_4$-$MgAl_2O_4$, $FeFe_2O_4$-$FeAl_2O_4$, and $FeFe_2O_4$-$MgAl_2O_4$) only two have been experimentally determined. They are the $FeFe_2O_4$-$MgAl_2O_4$ series published by Atlas and Sumida (1958) and the $MgFe_2O_4$-$MgAl_2O_4$ series by Rait (1946). Rait (1946) showed that a plot of cell dimensions against composition in mole percent for the $MgFe_2O_4$-$MgAl_2O_4$ series approaches a straight line, but the cell dimensions for the two end members do not agree with the present work, that of Paladino (1960), or that of Swanson and Fugar (1953). For this reason Rait's data have not been shown on figure 4. It has been assumed that the other series obey Vegard's law (Vegard, 1921) and are straight lines or at least fall within the two curves which are shown. This is probably a reasonable assumption as shown by the experimentally determined $FeFe_2O_4$-$FeAl_2O_4$ series and the $MgFe_2O_4$-$MgAl_2O_4$ series. When the (311) "d" spacing of a spinel is plotted on figure 4 a range of Al_2O_3 content in the spinel phase can be found.

EXPERIMENTAL RESULTS

General Statement

For the systematic study of a quinary system it is a virtual requirement that information be available for the limiting quaternary systems. Phase relations in four of the five limiting quaternary systems are especially relevant to the study of the quinary system Mg_2SiO_4-FeO-Fe_2O_3-$CaAl_2Si_2O_8$-SiO_2. The fifth limiting quaternary system, Mg_2SiO_4-FeO-Fe_2O_3-$CaAl_2Si_2O_8$, is too low in silica to be of general interest in petrology and is not considered in the present study.

The Mg_2SiO_4-FeO-Fe_2O_3-SiO_2 quaternary system has been described by Muan and Osborn (1956), and certain phase relations are shown in figures 1 and 2. The $CaAl_2Si_2O_8$-FeO-Fe_2O_3-SiO_2 system can be investigated in a manner similar to that employed by Muan and Osborn. Our data for this system are presented below. The Mg_2SiO_4-FeO-$CaAl_2Si_2O_8$-SiO_2 and the Mg_2SiO_4-Fe_2O_3-$CaAl_2Si_2O_8$-SiO_2 systems differ from the

other limiting systems in having only one of the iron oxides as a component. They represent in effect the quinary system at limiting conditions of pO_2. An estimate of phase relations for these two systems is obtained by extrapolating our data for the quinary system at the highest pO_2 used (air $= 10^{-0.7}$ atm) and at the lowest pO_2 used (10^{-11} atm) respectively.

The System $CaAl_2Si_2O_8$-FeO-Fe_2O_3-SiO_2

General statement.—The system $CaAl_2Si_2O_8$-FeO-Fe_2O_3-SiO_2 is sketched as a tetrahedron in figure 5a, on the faces and in the interior of which are shown univariant curves. Phase relations on the base of the tetrahedron, the system FeO-Fe_2O_3-SiO_2, are as reported by Muan (1955). Relations shown on the left face (Schairer, 1942) are a projection onto this

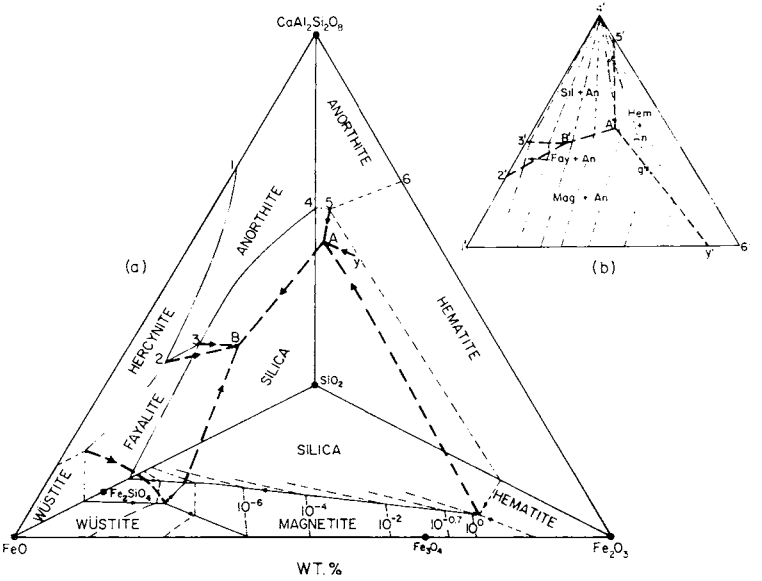

Fig. 5. Diagrams illustrating liquidus phase relations in the FeO-Fe_2O_3-$CaAl_2Si_2O_8$-SiO_2 system.

(a) System shown as tetrahedron with liquidus phase relations indicated. Light dashed and light solid lines are boundary curves on the three bounding faces. Dash-dot lines on the base are curves of constant pO_2 in atm. Heavy dashed lines within the tetrahedron are univariant curves along which three crystalline phases and a liquid phase are in equilibrium. The univariant curve y-A originates in the front face. The left face of the tetrahedron where phase relations are those in equilibrium with metallic iron is after Schairer (1942), and the base is after Muan (1955). Phase relations for the right face are inferred. Two liquid areas and the field of metallic iron are not shown.

(b) Anorthite-saturation plane. This diagram is a projection onto the base of the tetrahedron of the quaternary liquidus surface in equilibrium with anorthite and one or more other crystalline phases. The symbols 1′, 2′, 3′, 4′, 5′, 6′, A′, B′, y′ correspond to the same symbols without primes in figure 5a. Points f′ and g′ correspond to points f and g in figure 7. The heavy dashed lines are the same as those in figure 5a. The dash-dot lines are curves of constant pO_2 drawn schematically to represent the intersection of planes of constant pO_2 (not shown) in the tetrahedron with the anorthite-saturation surface.

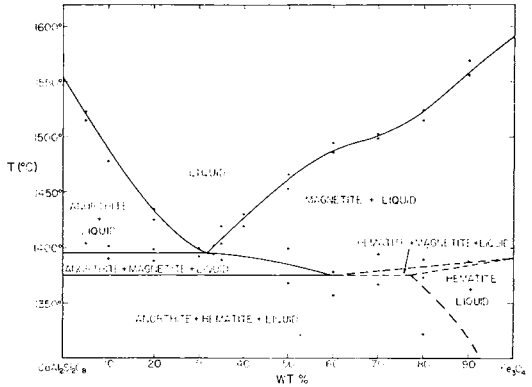

Fig. 6. Diagram illustrating phase equilibrium relations at $pO_2 = 10^{-0.7}$ atm (air) for the $CaAl_2Si_2O_8$-FeO-Fe_2O_3 system with all iron oxide calculated as Fe_3O_4. Dots represent especially significant experimental runs (see also table 1).

face of the metallic iron saturation surface. The right face represents liquid compositions at very high pO_2's. We have estimated positions of univariant curves for this face by extrapolation from the air-isobaric surface within the tetrahedron. The front face is not shown, but we do show a univariant line which originates in the front face at point y and extends to the invariant point A. Sketched within the tetrahedron are approximate locations of univariant lines drawn from the data described in the next section.

This system was studied only in air. Phase relations were therefore determined only for the isobaric surface at $pO_2 = 10^{-0.7}$ atm. This surface if shown in figure 5a would appear as an irregular surface having the SiO_2-$CaAl_2Si_2O_8$ join as one edge and extending from $10^{-0.7}$ isobar on the base up through the tetrahedron to the $CaAl_2Si_2O_8$ apex. It would lie close to the triangular plane, $CaAl_2Si_2O_8$-Fe_3O_4-SiO_2, as shown by the FeO/Fe_2O_3 weight ratios of liquid compositions listed in table 2. It is convenient for presentation of the data to recalculate all iron oxide as Fe_3O_4 so that points on the isobaric surface lie on this plane. Redrawn as an equilateral triangle, this plane showing phase relations at $pO_2 = 10^{-0.7}$ atm is pictured in figure 7. Phase relations for compositions at higher pO_2's than that of air—the region of figure 5 between the air-isobar and the right face—are of little interest in geology.

The system $CaAl_2Si_2O_8$-FeO-Fe_2O_3 in air.— Liquidus phase relations for the $CaAl_2Si_2O_8$-FeO-Fe_2O_3 system, the front face of figure 5a, have been experimentally determined at a constant pO_2 of $10^{-0.7}$ atm (air). The data are listed in table 1, and the liquid compositions are recalculated so that they lie on the $CaAl_2Si_2O_8$-Fe_3O_4 join as shown in figure 6. Four condensed phases are found to coexist along this join: liquid, magnetite, hematite, and anorthite. If the phase relations for the $CaAl_2Si_2O_8$-FeO-Fe_2O_3 system were ternary there would be a maximum of two condensed phases which could coexist with vapor over a range of

temperature at a constant pO_2. As is seen on figure 6 however, there are portions of this system at lower temperatures where three condensed phases coexist in equilibrium over a range of temperature. The reason for this deviation from ternary behavior is that Al_2O_3 and a very small amount of CaO (Phillips and Muan, 1958) enter the Fe_3O_4 structure, and Al_2O_3 enters the Fe_2O_3 structure. In addition, Fe^{+3} and Fe^{+2} may enter the anorthite structure, but the amount is small as indicated by refractive indices of the anorthite crystals and phase relations. The deviation from ternary behavior is small at the higher anorthite concentrations and becomes appreciable at high iron oxide compositions. Anorthite, hematite, and liquid coexist over a range of temperature, the lower limit of which was not determined.

The amount of Al_2O_3 in the magnetite and hematite structures was found by the procedure outlined in an earlier section and is shown in tables 7 and 8. The Al_2O_3 content of the spinels on the $CaAl_2Si_2O_8$-Fe_3O_4 join shown in table 7 was determined directly from the curve of Atlas and Sumida (1958).

The system $CaAl_2Si_2O_8$-FeO-Fe_2O_3-SiO_2 *in air.*—Phase equilibrium relations at liquidus temperatures for the system $CaAl_2Si_2O_8$-FeO-Fe_2O_3-SiO_2 at $pO_2 = 10^{-0.7}$ atm (air) are represented on the triangular plane

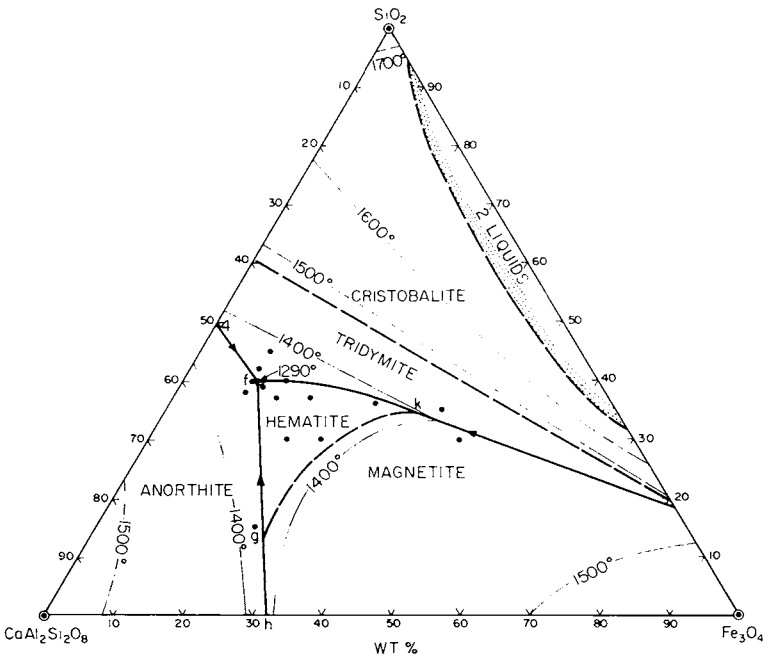

Fig. 7. Diagram illustrating phase equilibrium relations at $pO_2 = 10^{-0.7}$ atm (air) for the system $CaAl_2Si_2O_8$-FeO-Fe_2O_3-SiO_2 represented as an isobaric plane with all iron oxide calculated as Fe_3O_4. Heavy lines are boundary curves and light lines are isotherms on the liquidus surface. Dots are compositions used in the quenching experiments. Points f and g correspond to points f′ and g′ in figure 5b.

shown as figure 7, and the data are listed in table 2. This isobaric plane was constructed by calculating all iron oxide as Fe_3O_4. The liquidus surface is divided into four primary phase fields: anorthite, silica, hematite, and magnetite. The temperature of the phase boundary between the two iron oxide phases, hematite and magnetite, changes slightly with composition. This boundary has been dashed because the temperature change and its position have not been thoroughly investigated. The phase boundary representing the cristobalite-tridymite inversion temperature has been shown as 1470° after Fenner (1913). The samples containing silica which were X-rayed always contained cristobalite even though the temperature of the run was below 1470°. Samples containing crystalline SiO_2 as a phase are simply listed in table 2 as containing "silica". The boundary of the region of two liquids has been dashed in figure 7 because it was not experimentally investigated.

The composition of the point f, at 1290°, where liquid, silica, anorthite, and hematite are in equilibrium, is in weight percent: 11 iron oxide (calculated as Fe_3O_4), 39 SiO_2, and 50 $CaAl_2Si_2O_8$. The system deviates considerably from quaternary behavior as magnetite and hematite both contain Al^{+3} in their structures (for hematite see table 8) and liquid is a stable phase below 1290° over a range of temperature at the fixed pO_2.

The System Mg_2SiO_4-FeO-Fe_2O_3-$CaAl_2Si_2O_8$-SiO_2

General statement.—The system Mg_2SiO_4-FeO-Fe_2O_3-$CaAl_2Si_2O_8$-SiO_2 can, as discussed earlier, be systematically studied at a fixed pO_2 and then described and portrayed very much in the manner that a quaternary system is ordinarily treated. This is the approach used in this investigation. A series of tetrahedra have been developed representing phase relations in the system at a series of pO_2's. The results of studies in an air atmosphere will be described first, followed by those at lower pO_2's. Finally, the data will be depicted in a single anorthite-saturation tetrahedron.

The system Mg_2SiO_4-FeO-Fe_2O_3-$CaAl_2Si_2O_8$-SiO_2 in air. — Phase relations in the quinary system at $pO_2 = 10^{-0.7}$ atm (air) can be described by use of a tetrahedron as discussed earlier in referring to figure 3. The interior of this tetrahedron (fig. 3) has been investigated by studying mixtures lying on planes of constant anorthite content, that is, planes parallel to the base. Liquidus phase relations in an air atmosphere on the 40, 46, 48, and 50 weight percent anorthite planes are shown in figure 8. Data obtained on these planes and on intermediate planes are summarized in table 3. From the positions of phase boundaries and piercing points on these planes, a good estimate of the locations of univariant lines and invariant points in the tetrahedron can be obtained. These are shown in figure 9.

There are three liquidus points within the isobaric tetrahedron, P, E, and J (fig. 9 and table 9) at which four crystalline phases and a gas phase of $pO_2 = 10^{-0.7}$ atm are in equilibrium with the liquid. If

the phase relations were truly quinary, six phases could coexist at equilibrium at only a single temperature at a constant pO_2. They were however found to coexist over a range of temperature below 1185° (point E in fig. 9), as expected in view of the situation at point f mentioned in the previous section. Because of the difficulty in detecting small amounts of liquid, the range in temperature is not precisely known but is thought to be less than 30° for geologically important mixtures.

Of the six crystalline phases in the system, only silica and anorthite are approximately constant in composition. Refractive index measurements on the pyroxenes indicate a maximum $FeSiO_3$ content of 8 weight percent. The amount of CaO and Al_2O_3 in the pyroxene could not be measured, but it is thought to be small on the basis of refractive index measurements. Olivine is high in Mg_2SiO_4, as determined by optical and X-ray measurements, having a maximum Fe_2SiO_4 content of 4 weight percent. The range in Al_2O_3 content of the spinel phase is given in table 7.

The system Mg_2SiO_4-FeO-Fe_2O_3-$CaAl_2Si_2O_8$-SiO_2 at lower oxygen pressures.—Mixtures in the quinary system were run at pO_2's of 10^{-7},

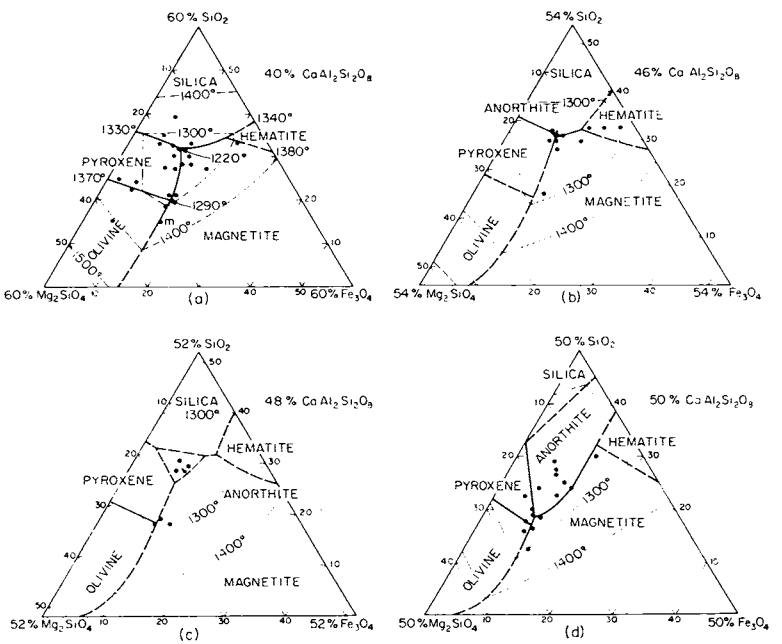

Fig. 8. Phase relations on planes of different $CaAl_2Si_2O_8$ content at $pO_2 = 10^{-0.7}$ atm (air) for the quinary system. Heavy lines are traces of divariant surfaces within the tetrahedron of figure 9. Light lines are liquidus isotherms. The composition of mixtures used in the quenching experiments, which lie on these planes, are shown by dots (see table 3). All iron oxide is calculated as Fe_3O_4 for plotting points on these isobaric planes.

(a) 40 wt percent $CaAl_2Si_2O_8$ plane, (b) 46 wt percent $CaAl_2Si_2O_8$ plane, (c) 48 wt percent $CaAl_2Si_2O_8$ plane, (d) 50 wt percent $CaAl_2Si_2O_8$ plane.

10^{-9}, and 10^{-11} atm as well as $10^{-0.7}$ atm. Liquidus phase relations at each of these partial pressures are sketched within the isobaric tetrahedra of figure 10. All iron oxide is calculated as Fe_3O_4 in (a), (b), and (c) and as FeO in (d). Tetrahedron (a) is redrawn after figure 9. For tetrahedra (b), (c), and (d) the left face in each case is after Andersen (1915). Relations on the base in (b) and (c) are estimated from data of Muan and Osborn (1956) and for the right face are inferred. The base and right face of (d), after Bowen and Schairer (1935) and Schairer (1942) respectively, represent phase relations for liquids in equilibrium with metallic iron. These low pO_2's are slightly lower than 10^{-11} atm. Data for the interior phase relations of (b), (c), and (d) were obtained at the indicated, fixed pO_2 and are listed in tables 4, 5, and 6. Some representative values of the ferrous to ferric ratios in the samples are shown in table 10.

The data listed in tables 4, 5, and 6 are for a range of $CaAl_2Si_2O_8$ contents from 30 to 51 weight percent. From these data triangular planes showing phase relations at various $CaAl_2Si_2O_8$ contents can be

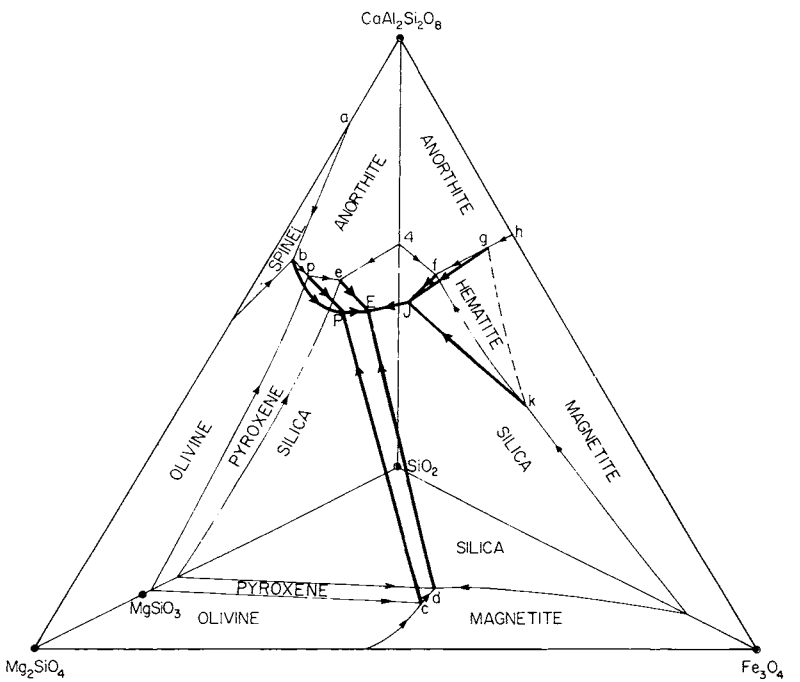

Fig. 9. Tetrahedron representing liquidus phase relations in the Mg_2SiO_4-FeO-Fe_2O_3-$CaAl_2Si_2O_8$-SiO_2 system at a constant pO_2 of $10^{-0.7}$ atm (air). Light lines are boundary curves on three of the four bounding isobaric planes. Heavy solid lines within the tetrahedron represent liquid compositions in equilibrium with three crystalline phases and a gas phase of $pO_2 = 10^{-0.7}$ atm. Arrows indicate the direction of decreasing temperature. Points P, E, and J are liquid compositions coexisting with four crystalline phases and a gas phase of $pO_2 = 10^{-0.7}$ atm (see table 9).

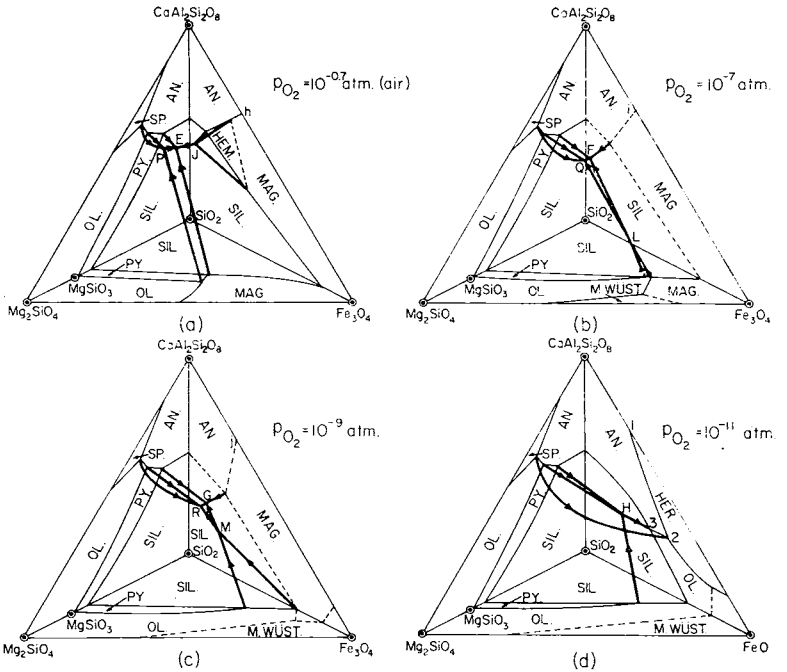

Fig. 10. Tetrahedra representing liquidus phase relations in the Mg_2SiO_4-FeO-Fe_2O_3-$CaAl_2Si_2O_8$-SiO_2 system at four different oxygen partial pressures. For plotting purposes, iron oxide is calculated as Fe_3O_4 in (a), (b), and (c) and as FeO in (d). Figure (a) is redrawn from figure 9 for ready comparison with (b), (c), and (d).

(a) $pO_2 = 10^{-0.7}$ atm (air), (b) $pO_2 = 10^{-7}$ atm, (c) $pO_2 = 10^{-9}$ atm, (d) $pO_2 = 10^{-11}$ atm.

Abbreviations used are: AN = anorthite, Sp = spinel ($MgAl_2O_4$), HEM = hematite with Al_2O_3 in solid solution, OL = olivine, PY = pyroxene, SIL = silica, M. WÜST = magnesiowüstite, MAG = magnetite with Mg^{+2} and Al^{+3} in solid solution, HER = hercynite.

sketched. The plane at 40 percent $CaAl_2Si_2O_8$ (14.7 percent Al_2O_3) which passes through the composition region of the invariant[4] points E, F, G, and H (fig. 10 and table 9) has been selected for illustrating phase relations on such planes. The relations at this $CaAl_2Si_2O_8$ content at different pO_2's are illustrated by the diagrams of figure 11. Comparison of the 40 percent $CaAl_2Si_2O_8$ planes (fig. 11) for $10^{-0.7}$, 10^{-7}, 10^{-9}, and 10^{-11} atm shows a marked and significant change in the phase relations as a function of pO_2. As pO_2 decreases, the primary phase volume of hematite disappears, that of magnetite becomes smaller, and those of pyroxene, anorthite, and olivine become larger. Minimum liquidus temperatures are lowered

[4] It is convenient to refer to these points of coexistence of six phases at constant pO_2 as "invariant" points, and lines of coexistence of five phases at constant pO_2 as "univariant" lines, just as the system MgO-FeO-Fe_2O_3-$CaAl_2Si_2O_8$-SiO_2 is called quinary throughout this paper, as explained in the introduction. The six phases are in equilibrium over a range of temperature instead of at a single-temperature, reflecting the deviation of the system from quinary behavior.

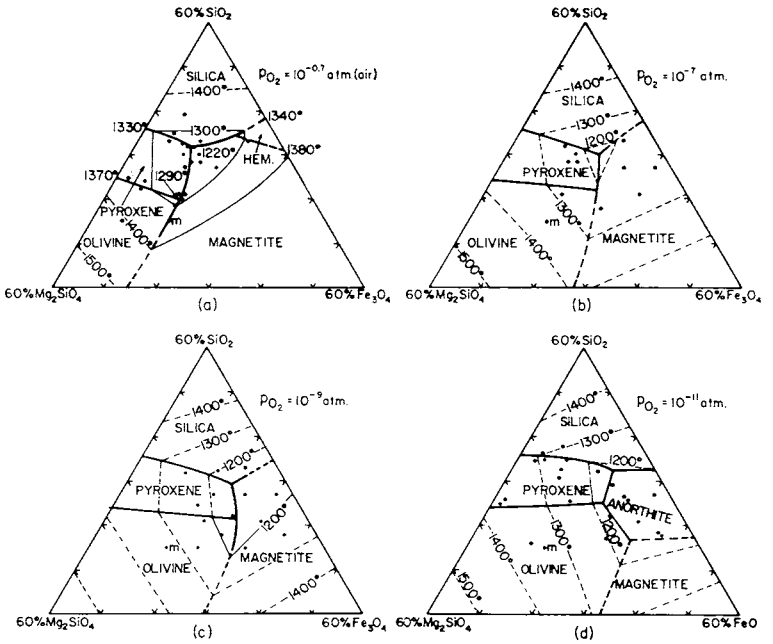

Fig. 11. Diagrams illustrating liquidus phase relations at a constant $CaAl_2Si_2O_8$ content of 40 wt percent at four different oxygen partial pressures in the Mg_2SiO_4-FeO-Fe_2O_3-$CaAl_2Si_2O_8$-SiO_2 system. These planes intersect the four isobaric tetrahedra of figure 10 at 40 wt percent $CaAl_2Si_2O_8$. Mixtures used in the experimental study lying within $\pm$ 2 percent of the 40 percent $CaAl_2Si_2O_8$ planes are shown by dots.

(a) $pO_2 = 10^{-0.7}$ atm (air), (b) $pO_2 = 10^{-7}$ atm, (c) $pO_2 = 10^{-9}$ atm, (d) $pO_2 = 10^{-11}$ atm.

and shifted toward higher iron oxide compositions. At approximately 10^{-9} atm the anorthite primary phase volume intersects the 40 percent $CaAl_2Si_2O_8$ plane as the anorthite volume expands downward into the tetrahedron with decreasing pO_2. On diagram (c) of figure 11 anorthite is not shown for although a very small anorthite field may exist on this plane, this could not be definitely established. At 10^{-11} atm the anorthite field is large, separating pyroxene and magnetite. On this plane (fig. 11d), therefore, anorthite and pyroxene coexist and also anorthite and magnetite, but pyroxene and magnetite whose fields adjoin at pO_2's of 10^{-9} and greater (fig. 11a, b, and c) are no longer compatible phases.

The tetrahedron for constant $pO_2 = 10^{-0.7}$ (fig. 10a) contains three invariant points, P, E, and J. Composition and temperature data for these points are listed in table 9. Each point represents the composition of a liquid in equilibrium with four crystalline phases and a gas phase of $pO_2 = 10^{-0.7}$ atm. Liquid P coexists with olivine, pyroxene, magnetite, and anorthite; liquid E with pyroxene, magnetite, tridymite and anorthite; liquid J with magnetite, hematite, tridymite, and anorthite. With lowered pO_2 the hematite phase volume

disappears. At 10^{-7} atm (fig. 10b) a point corresponding to J does not exist, but a new point L is present, representing a liquid that can coexist with olivine, magnetite, silica, and pyroxene. Points Q and F at 10^{-7} atm and R and G at 10^{-9} atm correspond to P and E in type of phase assemblage, but as the pO_2 is lowered the compositions of the liquid decrease in $CaAl_2Si_2O_8$ and increase in iron oxide contents. At some low pO_2 between 10^{-9} and 10^{-11} atm the points R and G merge with a point M to form two new points. This change in configuration of the invariant points is especially significant from the standpoint of pyroxene-magnetite relations. At and above 10^{-9} atm pyroxene and magnetite are compatible phases, coexisting with anorthite and with liquid compositions along the boundary curves P-E, Q-F, and R-G. At 10^{-11} atm (fig. 10d), however, pyroxene and magnetite are incompatible phases. Similarly, magnetite and silica become incompatible phases between 10^{-9} and 10^{-11} atm. At these low pO_2's the magnetite phase approaches hercynite in composition. At the very low pO_2 represented by figure 10d only one invariant point remains. Pyroxene, anorthite, olivine, and silica coexist at equilibrium with liquid of composition H.

At a high pO_2 (air) the lowest liquidus temperature is at point E (fig. 10a). As the pO_2 is lowered this point changes composition and its liquidus temperature (table 9) drops. Continued lowering of the pO_2 not only changes the temperature and composition of the invariant points but changes the whole configuration of the liquidus. The liquidus of some mixtures is raised (most of those in the primary phase field of anorthite) and that of others is lowered, while for some mixtures the liquidus is lowered and then raised because of a change in the primary crystalline phase. Examination of the direction (indicated by arrows) of the temperature drop shows that at a low pO_2 the minimum liquidus temperature is on the right-hand face of the tetrahedron (point 3, fig. 10d).

THE ANORTHITE-SATURATION TETRAHEDRON

From the tetrahedra of figure 10, a picture can be obtained of courses of crystallization of mixtures at different levels of pO_2, but courses of crystallization within each tetrahedron can be considered only under the condition of *constant* pO_2. During constant pO_2 crystallization of a mixture the oxygen content changes, as the system is open with respect to oxygen. We want also to be able to describe courses of crystallization under another type of condition and one no doubt more generally familiar to the reader because it applies when considering crystallization in the usual condensed silicate system, as for example in the treatment of courses of crystallization in the MgO-FeO-SiO_2 system by Bowen and Schairer (1935). In this case a crystallizing mixture is considered to have a *constant bulk composition*. The system is closed. During crystallization of a mixture the equilibrium pO_2 changes but not the total oxygen content.

One method of representing the liquidus phase relations under conditions of variable pO_2 in a three dimensional diagram is to control

arbitrarily some other parameter. For our purposes it is convenient and instructive to use the concentration of the $CaAl_2Si_2O_8$ (anorthite) component as this other parameter, restricting the manner of variation of the concentration at a level such that the liquid phase is always saturated with respect to anorthite.

This condition might be achieved experimentally if phase relations in the system MgO-FeO-Fe_2O_3-SiO_2 were determined using crucibles of $CaAl_2Si_2O_8$ with runs of sufficient length that the melts come into equilibrium with the crucible material—analogous to the studies of Bowen and Schairer (1935) of the MgO-FeO-SiO_2 system where iron crucibles were used and melts were all equilibrated with metallic iron. In this latter case only the part of the quaternary system Mg-Fe-Si-O was studied that has metallic iron as a constant crystalline phase in equilibrium with liquid. With this restriction the quaternary system was treated as the system MgO-FeO-SiO_2. Similarly we may select only that part of the quinary system MgO-FeO-Fe_2O_3-$CaAl_2Si_2O_8$-SiO_2 that has anorthite as a phase in equilibrium with liquid and then treat this as the system MgO-FeO-Fe_2O_3-SiO_2.

Instead, however, of using crucibles of $CaAl_2Si_2O_8$ in these studies, diagrams to show relations for the quinary system with anorthite always present as a phase are produced by a projection analogous to the projection of a surface of constant pO_2. A diagram for part of the quaternary system FeO-Fe_2O_3-$CaAl_2Si_2O_8$-SiO_2 (fig. 5) will be used to illustrate this type of projection. In the tetrahedron of figure 5, phase boundaries on the faces are shown by light solid and dashed lines, and quaternary univariant lines within the tetrahedron are indicated by heavy dashed lines. On the base the dot-dash lines are lines of constant pO_2.There are two quaternary invariant points A and B. An irregular surface can be visualized within the tetrahedron connecting the compositions of all liquids saturated with respect to anorthite and one or more other crystalline phases. The points 1-2-3-4-5-6-A-B-y all lie on such a surface. Inasmuch as this surface represents liquid compositions saturated with anorthite (and also one or more other crystalline phases) it will be called an anorthite-saturation surface. This surface can be projected from the anorthite apex onto the base of the tetrahedron to give an anorthite-saturation plane as shown in figure 5b. A point in the projection (fig. 5b) corresponding to a point in the tetrahedron is shown with a prime. Every point on this anorthite-saturation plane represents the composition of the liquid in terms of the ratio of SiO_2 to FeO to Fe_2O_3 exclusive of the percentage of $CaAl_2Si_2O_8$ in the liquid. The percentage of $CaAl_2Si_2O_8$ in the liquid is variable on the anorthite-saturation surface as can be seen from the difference in $CaAl_2Si_2O_8$ content of points 1 and 2 of figure 5a. Sets of contours on the anorthite-saturation plane could be used to represent lines of equal $CaAl_2Si_2O_8$ content of the liquid and of equal pO_2. We have not undertaken to draw on figure 5b the lines of equal $CaAl_2Si_2O_8$ content of the liquid but do show schematically lines of constant pO_2. As stated above every point on the projected anorthite-

saturation surface (fig. 5b) represents the composition of a liquid in equilibrium with anorthite and at least one other crystalline phase. The boundary lines of figure 5b represent liquid compositions in equilibrium with two crystalline phases plus anorthite, and the points of intersection of the boundary lines represent liquid compositions in equilibrium with three crystalline phases plus anorthite. Thus equilibrium phase relations in a quaternary system where the liquid is always in equilibrium with anorthite as one of the crystalline phases can be represented on a plane, and the concentration of anorthite in the liquid and of oxygen in the gas can also be shown.

The same approach will be used in showing phase relations for the more complicated quinary system Mg_2SiO_4-FeO-Fe_2O_3-$CaAl_2Si_2O_8$-SiO_2. The anorthite-saturation plane shown as figure 5b is one of four limiting anorthite-saturation planes of an anorthite-saturation volume for the quinary system, or in other words, the triangle of figure 5b is one face of an anorthite-saturation tetrahedron for the quinary system. By using an anorthite-saturation tetrahedron, it will be possible to represent graphically a part of the five component system as a function of pO_2. It will also be possible to compare the liquidus phase relations of the MgO-FeO-Fe_2O_3-SiO_2 system with those for the MgO-FeO-Fe_2O_3-SiO_2-$CaAl_2Si_2O_8$ system.

An anorthite-saturation plane can be developed from each of the tetrahedra of figure 10 by projecting from the $CaAl_2Si_2O_8$ apex onto the base the surface separating the anorthite primary phase volume from the rest of the tetrahedron. The planes resulting from these projections are shown in figure 12. Lettered and numbered points on figures 9 and 10 appear with primes on figure 12. The letters and numbers on figure 12a are taken from figure 9, an enlarged version of figure 10a, and primes added indicating that the points are projected. The designations, 4, e, p, b and a, on figure 9 appear, with primes, on all four triangles of figure 12 inasmuch as these points all lie on the Mg_2SiO_4-$CaAl_2Si_2O_8$-SiO_2 face which is common to all four of the tetrahedra of figure 10. Each of the planes of figure 12 represents the projected liquid compositions in equilibrium with anorthite and one or more other crystalline phases in terms of the ratio of Mg_2SiO_4 to Fe_3O_4 to SiO_2 exclusive of the silica in $CaAl_2Si_2O_8$. The actual percentage of $CaAl_2Si_2O_8$ in the liquid of the anorthite-saturation surface is given by the dashed-line $CaAl_2Si_2O_8$ contours.

The planes of figure 12, which show phase relations in the quinary system at four different pO_2's, were used in the construction of the anorthite-saturation tetrahedron of figure 13. This tetrahedron is an attempt to summarize in a single diagram general liquidus phase relations for that part of the quinary system in which anorthite crystals are present as a phase along with one or more other crystalline phases, a liquid phase, and a gas phase. In figure 13 each apex of the tetrahedron represents the composition of a liquid saturated with anorthite and has the composition

as given in the caption, with all iron oxide in the top apex calculated as Fe_3O_4 and in the bottom right apex as FeO.

This diagram (fig. 13) is helpful we believe in showing general phase relations for the quinary system but cannot be quantitatively used like the usual tetrahedron representing a quaternary system, for example, the tetrahedron of figure 1. The reason is that the $CaAl_2Si_2O_8$ content of liquids does not vary in a regular manner. Take for example the lower right edge, along which are points 1′, 2′, 3′, and 4′. The actual composition of these points can be read from figure 5a, except for the precise ratio of Fe_2O_3:FeO. Although the $CaAl_2Si_2O_8$ contents of points 1′ and 4′ (fig. 13) are 73 and 52 percent respectively, $CaAl_2Si_2O_8$ contents of points 2′ and 3′ do not lie between these two values but are considerably less than either. What does vary regularly from 1′ to 4′ along this edge of the tetrahedron is the $FeO:SiO_2$ *ratio,* exclusive of SiO_2 in the $CaAl_2Si_2O_8$ end member of the quinary system. Similarly the $Fe_3O_4:SiO_2$ ratio, exclusive of SiO_2 in $CaAl_2Si_2O_8$, varies regularly along the lines h′-4′ and h′-a′. Inasmuch as the iron oxide in liquid 1′ is nearly 100 percent FeO and that for point h′ has approximately a 1:1 Fe_2O_3:FeO ratio, points along 1′-h′ have a regularly changing $FeO:Fe_3O_4$ *ratio.* But we emphasize that the actual percentage of iron oxide changes

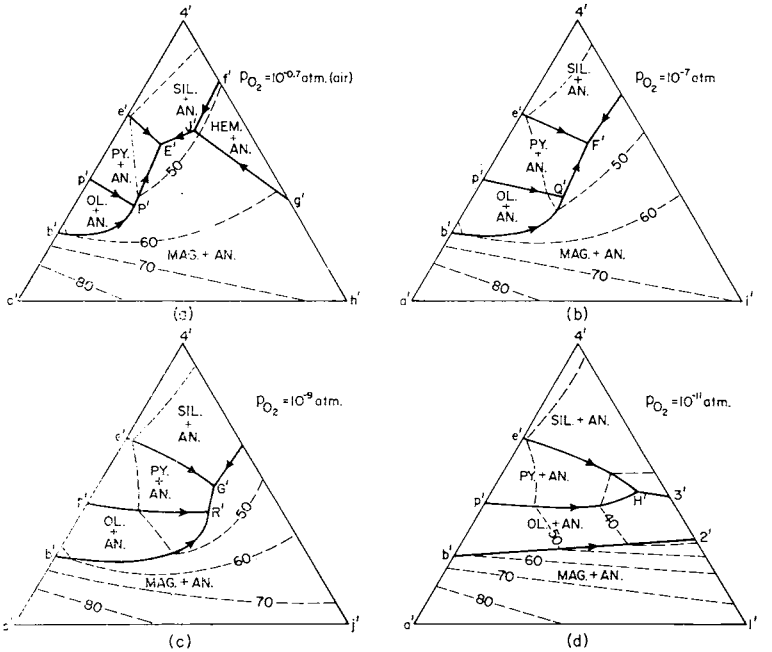

Fig. 12. Anorthite-saturation planes for the four isobaric tetrahedra of figure 10, developed by projecting the anorthite-saturation surface within each tetrahedron onto the base. Lettered and numbered points in figure 12 correspond to points similarly lettered in figures 9 and 10 but with a prime added to each. Dashed lines are contours of wt percent $CaAl_2Si_2O_8$ in the liquid phase.

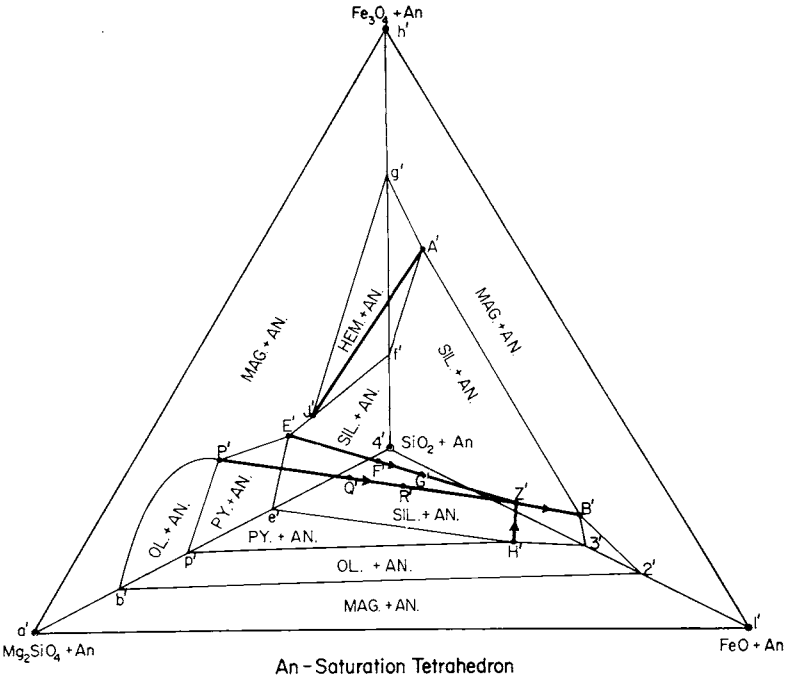

Fig. 13. Tetrahedral liquidus phase equilibrium diagram representing the anorthite-saturation volume for the system Mg_2SiO_4-FeO-Fe_2O_3-$CaAl_2Si_2O_8$-SiO_2. Apices are liquid compositions saturated with anorthite and one other crystalline phase and have compositions in wt percent as follows: top apex = 68 $CaAl_2Si_2O_8$, 32 iron oxide calculated as Fe_3O_4; right apex = 73 $CaAl_2Si_2O_8$, 27 iron oxide calculated as FeO; rear apex = 52 $CaAl_2Si_2O_8$, 48 SiO_2; left apex = 86 $CaAl_2Si_2O_8$, 14 Mg_2SiO_4. An = $CaAl_2Si_2O_8$.

The front face of the tetrahedron has been removed to show interior relations. The left face is the anorthite-saturation plane for air shown in figure 12a. The base of the tetrahedron is the anorthite-saturation plane for a $pO_2 = 10^{-11}$ atm shown in figure 12d. The right face is part of the anorthite-saturation plane of figure 5b. Heavy solid lines within the tetrahedron are univariant curves along which anorthite is in equilibrium with three other crystalline phases, liquid, and vapor. The two sets of points, Q′ and F′, and R′ and G′, correspond to these lettered points on anorthite-saturation surfaces at pO_2's of 10^{-7} and 10^{-9} atm respectively. These surfaces are shown projected onto the Mg_2SiO_4-Fe_3O_4-SiO_2 plane in figure 12b and c. The liquid of composition Z′ is in equilibrium with anorthite, pyroxene, olivine, tridymite, magnetite, and a gas phase having pO_2 of about 10^{-11} atm, at a temperature of 1075° ± 25°. Crystalline phases in equilibrium with liquid in the composition fields on each of the three faces of the tetrahedron are as indicated. AN = anorthite, MAG = magnetite, HEM = hematite, SIL = silica (tridymite), PY = pyroxene, OL = olivine.

irregularly along this line as the amount of $CaAl_2Si_2O_8$ required to saturate the liquid varies.

The left face and base of the tetrahedron of figure 13 are the isobaric anorthite-saturation planes of figure 12, a and d. The right face is taken from figure 5b. The univariant lines P′Q′R′Z′B′ and E′F′G′Z′B′ within the tetrahedron were constructed by drawing straight lines from P′ and E′ to a point Z′, above H′, and then continuing to B′. Although

schematic in this diagram, these lines represent real relations for the quinary system, giving a diagrammatic view of the manner of change of liquid compositions during crystallization. Temperatures and pO_2's decrease along these lines from left to right. Liquids along P'Q'R'Z' are in equilibrium with anorthite, olivine, pyroxene, magnetite, and vapor, along E'F'G'Z' are in equilibrium with anorthite, tridymite, pyroxene, magnetite, and vapor, and along Z'B' are in equilibrium with anorthite, olivine, tridymite, magnetite, and vapor. These univariant curves are very similar to the univariant curves in the tetrahedron of figure 1, but with anorthite present as a crystalline phase (fig. 13) temperatures along the lines are lower than in figure 1. Temperature and composition estimates for points P', E', F', G', B', and H' are listed in table 9.

DISCUSSION

Crystallization of Mixtures in the Quinary System, Mg_2SiO_4-FeO-Fe_2O_3-$CaAl_2Si_2O_8$-SiO_2

Crystallization of mixtures in the quaternary system MgO-FeO-Fe_2O_3-SiO_2 has been discussed in some detail in previous papers (Muan and Osborn, 1956; Osborn, 1959). Four types of crystallization were described: (1) equilibrium crystallization at constant total composition, (2) fractional crystallization at constant total composition, (3) equilibrium crystallization at constant pO_2, and (4) fractional crystallization at constant pO_2. From an understanding of courses of crystallization under these standard conditions, one can judge the nature of courses of crystallization under other pO_2 conditions, as for example increasing pO_2, and under varying degrees of fractionation. Although this quaternary system has here been expanded by the addition of $CaAl_2Si_2O_8$, the same principles apply. The problem is to be able to show the quinary system diagrammatically or otherwise to handle the data so that courses of crystallization can be treated. As pointed out in the preceding section, crystallization at constant pO_2 can be visualized with the aid of the isobaric tetrahedra of figure 10, while figure 13 has been developed as an aid for understanding crystallization at constant total composition. We will discuss briefly fractional crystallization under the two standard conditions.

Fractional crystallization at constant total composition.—The tetrahedron of figure 13 can be used very much as that of figure 1 for visualizing crystallization at constant total composition—the situation where the system is closed, where the oxygen content of a crystallizing mixture therefore does not change. Limitations in the use of figure 13 are: (1) anorthite must always be a crystalline phase present along with one or more of the other crystalline phases, (2) compositions of olivine, pyroxene, and magnetite cannot be readily shown, and (3) compositions of liquids cannot be read directly. Liquid compositions can be taken from this diagram only in terms of the ratio of Mg_2SiO_4:FeO:Fe_2O_3:SiO_2, exclusive of the SiO_2 tied up in the $CaAl_2Si_2O_8$ end member. The compositions of P', E', F', G', and B' however are known approximately

(table 9) along with the equilibrium pO_2 for each, so that compositions and pO_2's of other liquids can be estimated.

In looking briefly at fractional crystallization in this system let us consider the idealized condition of perfect fractionation. To illustrate this we will first take as an example a mixture with a composition lying on the curve P'Q'R'Z', say mixture Q' (fig. 13). The mixture Q' at the temperature of point Q' is at its liquidus temperature and is therefore just saturated with respect to AN, OL, PY, and MAG. As the temperature is lowered infinitesimally below that of Q', crystals of all four of these phases appear, causing the composition of the liquid to change. The composition of the liquid does not however move down P'Q'R'Z' because of the OL-PY reaction relation.[5] P'Q'R'Z' in other words is a reaction or peritectic line. The liquid can remain on this line during crystallization only if OL crystals are present to dissolve and only then if some degree of equilibrium crystallization is being considered. With perfect fractional crystallization a crystalline phase does not react with the liquid to dissolve but drops out of the system as far as any further reaction with the liquid is concerned. The liquid being considered therefore must leave the boundary curve P'Q'R'Z' immediately that crystals begin to separate. OL appears only as a trace. AN, PY, and MAG continue to precipitate as the temperature is lowered, causing the liquid to move along the boundary surface separating the PY + AN volume from the MAG + AN volume, the surface P'Q'R'Z'G'F'E', across to the E'F'G'Z' curve, intersecting this curve at a point below (to the right of) F'. The liquid composition must reach this second boundary curve at a point below F' because during crystallization of the mixture Q' at constant total composition the pO_2 decreases. The pO_2 of Q' and F' is the same, 10^{-7} atm. Crystals of SIL join AN, PY, and MAG in precipitating from the liquid as the liquid composition moves down E'F'G'Z' to Z'. As the liquid moves to Z' the PY phase[6] becomes more iron rich and the MAG decreases in MgO-content, although the percent of MgO in MAG is probably less than one percent at point F' as judged from Speidel's data (1964) for the system MgO-FeO-$Fe_2O_3SiO_2$. At point Z', OL with a high FeO-content appears as PY ceases to crystallize. With continued perfect fractionation the liquid approaches B' in composition. As the liquid moves from F' to B' the iron oxide content of the liquid

[5] The peritectic H' (fig. 13) lies on the silica side of the pyroxene join $MgSiO_3$-$FeSiO_3$ when this join is drawn on the base of the tetrahedron of figure 13, indicating a reaction relation between olivine and pyroxene for all compositions. This is contrasted with the simpler MgO-FeO-SiO_2 system (as shown on the base of fig. 1) which shows a reaction relation between olivine and pyroxene only at low iron-oxide concentrations. The addition of $CaAl_2Si_2O_8$ to the MgO-FeO-Fe_2O_3-SiO_2 system thus appears to increase the range of the olivine-pyroxene reaction relation as expected in view of the phase relations in the system Mg_2SiO_4-$CaAl_2Si_2O_8$-SiO_2 (left face of tetrahedron of fig. 10). This effect of anorthite in extending olivine-pyroxene reactions was remarked upon by Bowen and Schairer (1935, p. 211).

[6] There may be an invariant point along E'F'G'Z' at which two pyroxenes, anorthite, tridymite, and magnetite coexist with liquid and gas, but we have no data on this.

increases from 14 to 38 percent (table 9), and the pO_2 decreases from 10^{-7} to about 10^{-11} atm.

If we start with a mixture whose composition lies in the OL + AN volume, the course of fractional crystallization will be different during the early stages. As OL + AN separate the liquid will move to one of the surfaces bounding the OL + AN volume, p'P'Z'H', b'P'Z'B'2', or Z'B'3'-H', which one depending on initial liquid composition. If the initial liquid has a composition similar to that of an olivine basalt, the third crystalline phase will be either PY or MAG, the liquid will move to the E'F'G'Z'B' line, and with perfect fractionation will then move on down to B'. The path of the liquid in moving to the E'F'G'Z'B' line may be complicated in detail. For a description of this type of crystallization in similar but simpler systems, the reader is referred to thorough discussions by Bowen and Schairer (1935), Muan and Osborn (1956), and Osborn (1959).

If the composition of a mixture is such that the primary phase separating along with AN is one of PY or MAG or SIL, again the course of the liquid during perfect fractionation is to the E'F'G'Z'B' line and on down to B'. Therefore, whether the initial $FeO:Fe_2O_3$ ratio is high or low and irrespective of the crystalline phase first separating, the path of fractional crystallization is to B', a point of high iron oxide and low pO_2. If fractionation is not perfect, then the liquid composition will not move all the way to B', but the direction of its movement will be toward E'F'-G'Z'B' and then down this curve.

Fractional crystallization at constant pO_2.—If the *oxygen pressure* is held constant during crystallization (oxygen here considered as a mobile component), the *oxygen content* of a mixture will change, and for compositions similar to those of basalt and andesite, the oxygen content of condensed phases no doubt increases. The isobaric tetrahedra of figure 10 are useful in visualizing crystallization under these conditions. Here phase relations are indicated for four pO_2 levels. At the pO_2 of air figure 10a applies. This case has already been discussed (Osborn and Roeder, 1960) wherein phase relations in the tetrahedron were compared with those in the system represented by just the base of the tetrahedron. It is especially noteworthy that just as in the case described above, adding the anorthite composition to the system MgO-FeO-Fe_2O_3-SiO_2 does not change the nature of the courses of crystallization. With fractional crystallization at this constant pO_2, liquids move to the point E, an isobaric eutectic point.

At a lower pO_2 and one similar to that of basaltic magma, figure 10b applies. During the fractional crystallization of a mixture simulating olivine basalt in composition, the liquid moves to point F, increasing thereby in silica content. Just as in the case of figure 10a, relations are such at 10^{-7} atm (pO_2) that the pyroxene primary phase volume is truncated by that of magnetite, preventing liquids on fractional crystallization from moving very far down the boundary curve to higher iron oxide contents. Instead a liquid, with pryoxene as one of the phases

separating, moves only as far as the line QF or the face QLF and then must change abruptly in composition and move toward F, which is the direction of increasing silica with little or no increase in iron oxide. At the lower pO_2 of 10^{-9} atm, figure 10c applies, with point G corresponding to F of figure 10b.

At a pO_2 between 10^{-9} and 10^{-11} atm, the primary phase volumes of pyroxene and magnetite cease to adjoin. Therefore at lower pO_2's the liquid is not stopped at an isobaric eutectic (such as G) by the crystallization of an iron oxide phase, magnetite, but rather as can be seen from figure 10d the liquid moves during perfect fractionation to a point H and then along H-3 to high iron oxide contents. Magnetite does not appear at all as a phase during the crystallization of mixtures simulating basalts and andesites in composition at this very low pO_2 of 10^{-11} atm.

Significant iron enrichment can therefore occur in liquids of simplified olivine basalt composition fractionally crystallized under either one of two different types of conditions, illustrated for this quinary system by the two sketches, figure 13 and figure 10d. In the first, where total composition is constant, the pO_2 may be high, moderate, or low at the beginning of crystallization. If high or moderate, magnetite is an early phase; the liquid moves to the E'F'G'Z'B' line and then down to B' (fig. 13). Magnetite crystallization prevents the liquid from moving up into the tetrahedron to high Fe_2O_3/FeO ratios. If the pO_2 is initially low, magnetite is a late phase to separate. In the second case, illustrated by figure 10d, fractional crystallization at this very low but constant pO_2 can also develop an iron rich liquid, but here magnetite is not a phase separating from liquids of initial basalt type compositions.

Petrologic Implications

When the results of studies of the quaternary system MgO-FeO-Fe_2O_3-SiO_2 were applied to the problem of the crystallization and differentiation of basaltic magma (Osborn, 1959), the extrapolation was greater than might be desired, for lime, alumina, and alkalis were all absent from the simpler system. We have now in this quinary system added lime and alumina. They have been added in a ratio (1:1) which seems reasonable from the standpoint of application of results to basaltic magma. Liquid compositions in this system approach closely those of basalt and related magmas, and therefore application of phase relations can be more direct and certain than formerly. It is of especial importance then to note that the conclusions earlier drawn (Osborn, 1959), by applying results from the quaternary system to basaltic magma are not changed on the basis of this present work. We can now use figure 10b instead of figure 2 as formerly for illustrating phase relations at constant pO_2. The composition of F (fig. 10b and table 9) is that of the residual liquid on fractionally crystallizing a mixture in the system simulating olivine basalt in composition where the final $pO_2 = 10^{-7}$ atm. This is approximately the pO_2 of basaltic magma (Fudali, Muan, and Osborn, 1961). The andesite-like liquid, F, coexists with anorthite, pyroxene,

magnetite, and tridymite. Liquids of basalt-like composition in the system do not have to be extremely fractionated to reach this composition point, but the greater the degree of fractionation the higher the percent of liquid of composition F. During fractional crystallization of a basalt-like liquid in this system, pO_2 does not have to remain constant at 10^{-7} atm for the final liquid to have composition F; but if it does remain constant at 10^{-7} atm, or if the final $pO_2 = 10^{-7}$ atm, then the final liquid has the composition F. If during the fractional crystallization of a natural basaltic magma the pO_2 is maintained at about 10^{-7}, or if after crystallizing partly at a higher or lower or fluctuating pO_2 it levels off at a final pO_2 of about 10^{-7} atm, then except for the effect of alkalis and minor elements the liquid phase should be similar in composition to that of point F.

Similarly, figure 13 can now be used instead of figure 1 for illustrating phase relations under conditions of constant total composition. For any liquid in the compositional region of figure 13 similar to basalt, the residual liquid on fractional crystallization approaches the ferro-basalt type of composition of point B′ (fig. 13 and table 9), a liquid which coexists with anorthite, fayalite, magnetite, and tridymite.

It is clear from the diagrams of figures 10b and 13 that the initial $FeO:Fe_2O_3$ ratio is immaterial as far as residual liquid composition on fractional crystallization is concerned. Liquids move to and remain at F if pO_2 reaches and remains at 10^{-7} while liquid is still present. Liquids move down E′F′G′Z′B′ during fractional crystallization if pO_2 decreases as in a closed system.

Differences in final liquid composition on fractional crystallization at various conditions of pO_2 can be further illustrated by reference to figure 14. In this diagram are plotted the estimated compositions of liquids lying along the univariant curve E′F′G′Z′B′ of figure 13. Points E′, F′, G′, and B′ shown along the top of diagram, are the composition points appearing in figure 13. They represent final liquid composition on fractional crystallization of a simplified olivine basalt at pO_2's respectively of $10^{-0.7}$, 10^{-7}, 10^{-9}, and 10^{-11} atm. Thus for example the final liquid from fractional crystallization at $pO_2 = 10^{-0.7}$ atm contains 57 percent SiO_2 and 8 percent iron oxide whereas the final liquid at 10^{-9} atm contains 51 percent SiO_2 and 21 percent iron oxide. From the curves joining these points the final liquid composition can be estimated for fractional crystallization of a simplified olivine basalt at any pO_2 within the range shown. These curves also represent the change in composition of liquids moving down the curve E′F′G′Z′B′ of figure 13 during fractional crystallization under conditions of constant total composition. The composition of the simplified basalt, m, listed in table 9 has also been plotted in figure 14 (shown by X's). This composition was plotted at a $pO_2 = 10^{-8}$ atm which is in the range of pO_2's of natural basaltic magmas (Fudali, Osborn, and Muan, 1961; and also Heald, Naughton, and Barnes, 1963). If this simplified basalt is fractionally crystallized at a constant pO_2 of 10^{-8} atm the last liquid will contain approximately 54

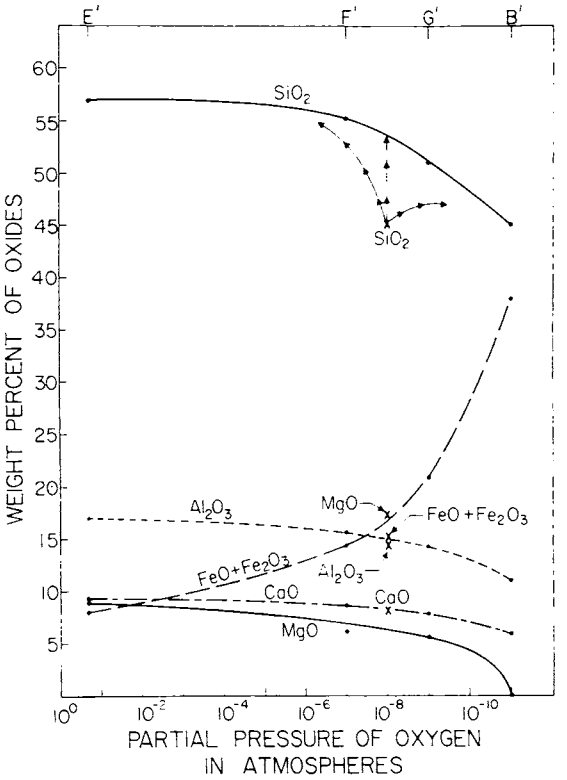

Fig. 14. Series of curves showing the change in composition of liquids along the E'F'G'Z'B' univariant curve in figure 13 as a function of pO_2. The X's represent the composition in wt percent of the oxides of a simplified basalt, m (figs. 8a and 11a and table 9), plotted at a pO_2 of 10^{-8} atm. The lines with arrows near the top of the diagram show the general silica trend of the liquid during fractional crystallization of this simplified basalt liquid at a constant pO_2 (vertical arrow), increasing pO_2 (left arrow), and decreasing pO_2 or constant total composition (right arrow).

percent SiO_2. The general silica trend is shown by the vertical arrowed line extending upward from the initial SiO_2 percent point for m of 45. If during crystallization the pO_2 should increase, a silica crystallization trend such as shown by the left-hand arrowed line might take place while with decreasing pO_2 a silica trend such as indicated by the right-hand arrowed line might occur. The change in liquid composition with respect to iron oxide, lime, alumina, and magnesia can be traced in a similar manner.

The SiO_2 curve in figure 14 rises from a low of 45 percent at the right end to a high of 57 percent at the left end. The SiO_2 content of all residual liquids from fractional crystallization at any pO_2 from $10^{-0.7}$ to 10^{-11} atm of all mixtures in the system of figure 13 lie as points on this line. Therefore the maximum SiO_2 content during fractional crystallization is 57 percent. As shown for mixture, m, in figure 14, the SiO_2 content

may remain about constant at 45 percent if fractionation is extreme and of the constant total composition type, for under these conditions pO_2 drops to 10^{-11} atm and the SiO_2 content changes as indicated schematically by the right arrowed line in figure 14. If $pO_2 = 10^{-8}$ atm at the close of crystallization, the residual liquid contains 54 percent SiO_2. Higher SiO_2 contents, but not greater than 57 percent unless pO_2 exceeds that of air ($10^{-0.7}$ atm), are attained if the final pO_2 is greater than 10^{-8} atm.

Inasmuch as liquids in this system closely approach basaltic magma in composition, how may residual liquids higher in SiO_2 than 57 percent, for example, dacitic or rhyolitic liquids, be formed by fractional crystallization of a basaltic or olivine basaltic magma? Higher SiO_2 residual liquids may form if alkalis are present—the principal oxide constituents of basaltic magma not present in the system discussed in this paper, CaO-MgO-FeO-Fe_2O_3-Al_2O_3-SiO_2. Alkalis added to this system should have little effect on the early stages of fractional crystallization of basalt-like liquids in the system, but as crystallization proceeds they will exert an increasingly important effect on the change in composition of the liquid. The most pronounced effect will be in causing the liquid to move to higher levels of SiO_2 than possible without the alkalis.

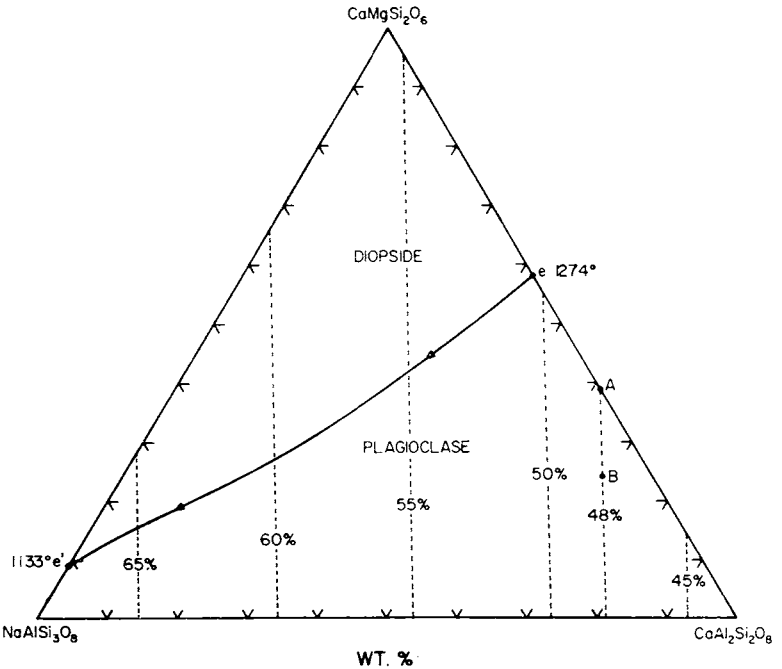

Fig. 15. Liquidus diagram of the $NaAlSi_3O_8$-$CaAl_2Si_2O_8$-$CaMgSi_2O_6$ system, after Bowen (1915), modified to conform to the recent experimental data of Schairer and Yoder (1960). Dashed lines are lines of constant silica content. Points A and B are referred to in text.

This effect of the alkalis may be illustrated by comparing the fractional crystallization of liquids A and B of figure 15. This diagram for the system $NaAlSi_3O_8$-$CaAl_2Si_2O_8$-$CaMgSi_2O_6$ is from the work of Bowen (1915), revised on the basis of later studies (Schairer and Yoder, 1960).[7] On fractional crystallization of composition A, anorthite separates causing the liquid to change composition to the minimum point e at 1274°. In so doing the liquid increases in SiO_2 from 48 percent to 51 percent. By adding a small amount of Na_2O to give composition B (0.8 percent Na_2O), the liquid on crystallization moves to and then down the boundary curve toward e′ at 1133°. With extreme fractionation the composition of the final liquid approaches that of e′. The SiO_2 content has now changed from 48 percent at B to 68 percent at e′. This simple model is presented to illustrate the effect of an addition of Na_2O in increasing the silica content of the liquid and decreasing the temperature of solidification during crystallization. These effects must also take place with the addition of Na_2O (and K_2O) to the quinary system MgO-FeO-Fe_2O_3-$CaAlSi_2O_8$-SiO_2.

Water present in the magma will also influence liquid compositions to change toward higher SiO_2 contents if during fractional crystallization temperatures drop low enough for crystallization of amphiboles and biotites, as discussed by Bowen (1922).

If we think in terms of reaction series as a scheme for illustrating courses of crystallization of basaltic magma (Bowen, 1922; Osborn, 1962), phase relations for the system discussed in this paper involve the olivine → pyroxene discontinuous reaction series and the magnetite continuous series but exclude the important continuous reaction series of the plagioclase feldspars and the hydrous members of the discontinuous series. Only the basic end member of the feldspar series, anorthite is present, and there is no water. Thus the SiO_2 enrichment of the residual liquid to a maximum of 57 percent is a result alone of the action of the anhydrous part of the discontinuous series plus magnetite and anorthite. With the SiO_2 enrichment effect of the plagioclase series, and of water, impressed on the course of change of liquid compositions during fractional crystallization, much higher SiO_2 contents may result.

ACKNOWLEDGMENTS

The writers wish to acknowledge the very helpful suggestions of Dr. J. W. Greig received during discussions of the manuscript with him. We wish also to thank the Bethlehem Steel Corporation and the New Mexico Institute of Mining and Technology for their financial support during the course of this experimental study.

[7] These more recent data show that the feldspar in equilibrium with diopside and liquid e′ is plagioclase rather than pure albite and that the diopside is aluminous. Liquid of composition e′ coexists with crystals of sodic plagioclase and diopside over the temperature range, 1133° to 1045°. The diopside in equilibrium with liquid e and anorthite is probably also aluminous as concluded by Osborn (1942).

References

Andersen, Olaf, 1915, The system anorthite-forsterite-silica: Am. Jour. Sci., 4th ser., v. 39, p. 407-454.

Atlas, L. M., and Sumida, W. K., 1958, Solidus, subsolidus, and subdissociation phase equilibria in the system Fe-Al-O: Am. Ceramic Soc. Jour., v. 41, p. 150-160.

Bowen, N. L., 1915, The crystallization of haplobasaltic, haplodioritic, and related magmas: Am. Jour. Sci., 4th ser., v. 40, p. 161-185.

———— 1922, The reaction principle in petrogenesis: Jour. Geology, v. 30, p. 177-198.

Bowen, N. L., and Andersen, Olaf, 1914, The binary system MgO-SiO_2: Am. Jour. Sci., 4th ser., v. 37, p. 487-500.

Bowen, N. L., and Schairer, J. F., 1935, The system MgO-FeO-SiO_2: Am. Jour. Sci., 5th ser., v. 29, p. 151-217.

Brown W. L., and Smith, J. V., 1963, High-temperature X-ray studies on the polymorphism of $MgSiO_3$: Zeitschr. Kristallographie, v. 118, p. 186-212.

Day, A. L., Shepherd, E. S., and Wright, F. E., 1906, The lime-silica series of minerals: Am. Jour. Sci., 4th ser., v. 22, p. 265-302.

Darken, L. S., and Gurry, R. W., 1945, The system iron-oxygen: I, The wüstite field and related equilibria: Am. Chem. Soc. Jour., v. 67, p. 1398-1412.

Fenner, C. N., 1913, The stability relations of the silica minerals: Am. Jour. Sci., 4th ser., v. 36, p. 381-384.

Fudali, R. F., Muan, Arnulf, and Osborn, E. F., 1961, Oxygen fugacities of basaltic magmas [abs.]: Geol. Soc. America Spec. Paper 68, p. 179-180.

Heald, E. F., Naughton, J. J., and Barnes, I. L., 1963, The chemistry of volcanic gases. 2. Use of equilibrium calculations in the interpretation of volcanic gas samples: Jour. Geophys. Research, v. 68, p. 545-557.

Hillebrand, W. F., Lundell, G. E. F., Bright, H. I., and Hoffman, J. I., 1953, Applied inorganic analysis, 2nd ed.: New York, John Wiley and Sons, Inc., 929 p.

Kennedy, G. C., 1955, Some aspects of the role of water in rock melts, *in* Poldervaart, Arie, ed., Crust of the earth—a symposium: Geol. Soc. America, Spec. Paper 62, p. 489-503.

Muan, Arnulf, 1955, Phase equilibria in the system FeO-Fe_2O_3-SiO_2: Am. Inst. Mining Engineers Trans., Jour. Metals, v. 203, p. 965-967.

———— 1958, Phase equilibria at high temperatures in oxide systems involving changes in oxidation states: Am. Jour. Sci., v. 256, p. 171-207.

———— 1961, A "new" crucible material for study of iron silicates: Am. Ceramic Soc. Jour., v. 44, p. 298.

Muan, Arnulf, and Gee, C. L., 1956, Phase equilibrium studies in the system iron oxide-Al_2O_3 in air and at 1 atm O_2 pressure: Am. Ceramic Soc. Jour., v. 39, p. 207-214.

Muan, Arnulf, and Osborn, E. F., 1956, Phase equilibria at liquidus temperatures in the system MgO-FeO-Fe_2O_3-SiO_2: Am. Ceramic Soc. Jour., v. 39, p. 121-140.

Osborn, E. F., 1942, The system $CaSiO_3$-diopside-anorthite: Am. Jour. Sci., v. 240, p. 751-788.

———— 1959, Role of oxygen pressure in the crystallization and differentiation of basaltic magma: Am. Jour. Sci., v. 257, p. 609-647.

———— 1962, Reaction series for subalkaline igneous rocks based on different oxygen pressure conditions: Am. Mineralogist, v. 47, p. 211-226.

Osborn, E. F., and Roeder, P. L., 1960, Effect of oxygen pressure on crystallization in simplified basalt system: Internat. Geol. Cong., 21st, Copenhagen, 1960, Rept., pt. 13, p. 147-155.

Paladino, A. E., 1960, Phase equilibria in the ferrite region of the system FeO-MgO-Fe_2O_3: Am. Ceramic Soc. Jour., v. 43, p. 183-191.

Phillips, Bert, and Muan, Arnulf, 1958, Phase equilibria in the system CaO-iron oxide in air and at 1 atm O_2 pressure: Am. Ceramic Soc. Jour., v. 41, p. 445-454.

Presnall, D. C., ms, 1963, The join Mg_2SiO_4-$CaMgSi_2O_6$-iron oxide at oxygen pressures from 0.21 to 10^{-8} atmospheres: Ph.D. thesis, The Penn. State Univ.

Rait, J. R., 1946, An X-ray investigation into the constitution of chrome ores; Third report on refractory materials: The Iron and Steel Inst., Spec. Rept. 32, p. 175-209.

Rankin, G. A., and Wright, F. E., 1915, The ternary system CaO-Al_2O_3-SiO_2: Am. Jour. Sci., 4th ser., v. 39, p. 1-79.

Richards, R. G., and White, J., 1954, Phase relationships of iron-oxide-containing spinels, Pt. I. Relationships in the system Fe-Al-O: British Ceramic Soc. Trans., v. 53, p. 233-270.

Roeder, P. L., ms, 1960, Phase relations in the Mg_2SiO_4-$CaAl_2Si_2O_8$-FeO-Fe_2O_3-SiO_2 system and their bearing on crystallization of basaltic magma: Ph.D. thesis, The Penn. State Univ.

Schairer, J. F., 1942, The system CaO-FeO-Al_2O_3-SiO_2: I, Results of quenching experiments on five joins: Am. Ceramic Soc. Jour., v. 25, p. 252.

Schairer, J. F., and Yoder, H. S., Jr., 1960, The nature of residual liquids from crystallization, with data on the system nepheline-diopside-silica: Am. Jour. Sci., v. 258-A (Bradley v.), p. 273-283.

Speidel, D. H., ms, 1964, Element distribution among coexisting phases in the system MgO-FeO-Fe_2O_3-SiO_2-TiO_2 as a function of temperature, oxygen fugacity, and bulk composition: Ph.D. thesis, The Penn. State Univ.

Swanson, H. E., and Fuyat, R. K., 1953, Standard X-ray diffractions powder patterns: Natl. Bur. Standards Circ. 539 II, p. 35-38.

Vegard, L., 1921, Die Konstitution der Misch-Kristalle and die Raummer Fullung der Atom: Annales Physik, v. 5, p. 17.

Wager, L. R., and Deer, W. A., 1939, Geological investigations in east Greenland, Pt. 3, The petrology of the Skaergaard intrusion, Kangerdlugssuag, east Greenland: Medd. om. Grønland, v. 105, 352 p.

Yoder, H. S., Jr., and Sahama, Th. G., 1957, Olivine X-ray determination curve: Am. Mineralogist, v. 42, p. 475-491.

APPENDIX

TABLE I

Results of quenching experiments at an oxygen partial pressure of $10^{-0.7}$ atm (air) for the system $CaAl_2Si_2O_8$-FeO-Fe_2O_3

Preparation no.	Composition (wt %) $CaAl_2Si_2O_8$	Composition (wt %) Fe as Fe_3O_4	Temp (°C)	Time (hr)	Phases present*
5	95.0	5.0	1523	2	L
			1515	1.5	An + L
			1404	16	An + L
6	90.0	10.0	1500	3.5	L
			1478	3	An + L
			1401	1.5	An + L
			1390	2	An + Mag + L
7	80.0	20.0	1434	2	L
			1425		An + L
			1398		An + L
			1388		An + Mag + L
8	70.0	30.0	1399	4	L
			1392	2	An + Mag + L
4	66.7	33.3	1401	14	L
			1399	5	Mag + L
			1394	4	Mag + An + L
16	65.0	35.0	1419	22	L
			1403	20	Mag + L
			1389	16	Mag + An + L
9	60.0	40.0	1430	2	L
			1419	2	Mag + L
3	50.0	50.0	1466	18	L
			1453	2.5	Mag + L
			1399	5	Mag + L
			1368	4.5	Hem + An + L
11	40.0	60.0	1494	16	L
			1486	1.5	Mag + L
			1378	23	Mag + L
			1357	24	Hem + An + L
12	30.0	70.0	1502	12	L
			1498	24	Mag + L
			1394	2.5	Mag + L
			1367	48	Hem + An + L
13	20.0	80.0	1524	2	L
			1515	6	Mag + L
			1389	17	Mag + L
			1373	12	Hem + L
			1322	3	Hem + An + L
14	10.0	90.0	1569	2	L
			1556	4	Mag + L
			1387	16.5	Mag + L
			1351	18	Hem + L

* Abbreviations in this and succeeding tables have the following meanings: L = liquid, An = anorthite, Mag = magnetite, Hem = hematite.

TABLE 2

Results of quenching experiments at an oxygen partial pressure of $10^{-0.7}$ atm (air) for the system $CaAl_2Si_2O_8$-FeO-Fe_2O_3-SiO_2

Preparation no.	Composition (wt %) $CaAl_2Si_2O_8$	Fe as Fe_3O_4	SiO_2	Temp (°C)	Time (hr)	Phases present*
39	25.0	40.0	35.0	1452	2	L
				1448	2	Sil + L
				1421	5	Sil + Mag + L
35	25.0	45.0	30.0	1389	20	Mag + L
				1362	3	Hem + Sil + L
34	34.0	30.0	36.0	1395	3	L
				1384	2	Hem + L
29	43.0	20.0	37.0	1376	17	L
				1368	3	Hem + L
				1302	2	Hem + L
26	45.0	10.0	45.0	1355	20	L
				1340	48	Sil + L
				1305	2	Sil + L
				1277	17	Sil + An + Hem + L
31	45.0	15.0	40.0	1358	12	L
				1348	3	Hem + Sil + L
				1311	18	Hem + Sil + L
				1279	2	Hem + Sil + An +L
27	45.0	25.0	30.0	1369	18	L
				1364	20	Hem + L
				1293	4	Hem + L
				1276	3	Hem + An + Sil + L
28	48.0	10.0	42.0	1339	2	L
		(0.45 at 1332°)**		1327	3	Sil + L
				1300	12	Sil + An (tr) + L
				1278	19	Sil + An + Hem + L
33	48.0	15.0	37.0	1307	4	Hem + L
				1297	4	Hem + Sil + An + L
32	49.0	12.0	39.0	1312	3	L
				1299	4	Hem + Sil + L
				1277	16	Hem + Sil + An + L
38	50.0	10.0	40.0	1313	19	An (tr) + L
				1305	17	An + Sil + L
				1287	19	An + Sil + Hem (tr) + L
30	50.0	20.0	30.0	1350	3	L
		(0.55 at 1335°)		1339	16	Hem + L
				1302	13	Hem + An + L
25	52.0	10.0	38.0	1315	17	L
		(0.52 at 1314°)		1307	4	An + Sil + L
				1288	3	An + Sil + Hem + L
36	62.0	23.0	15.0	1384	17	L
				1382	2	An + L
				1348	2	An + Hem + L

* Abbreviations used in this table and not explained previously have the following meanings: Sil = silica (tridymite), (tr) = trace.

** Numbers in parentheses show FeO:Fe_2O_3 ratio as determined by analysis of the mixture after quenching from the temperature as shown.

TABLE 3

Results of quenching experiments at an oxygen partial pressure of $10^{-0.7}$ atm (air) for the system Mg_2SiO_4-FeO-Fe_2O_3-$CaAl_2Si_2O_8$-SiO_2

Preparation no.	Composition (wt %)				Temp (°C)	Time (hr)	Phases present*
	$CaAl_2Si_2O_8$	Mg_2SiO_4	SiO_2	Fe as Fe_3O_4			
73	40.0	33.0	24.6	2.4	1352	16	L
					1348	5	Py (tr) + L
57	40.0	39.0	15.0	6.0	1284	2	Ol + L
59	40.0	31.8	22.2	6.0	1327	19	L
					1323	2	Ol + L
50	40.0	30.0	24.0	6.0	1314	2	L
					1309	3	Py + L
					1202	17	Py + An + Sil + L
51	40.0	21.0	33.0	6.0	1274	12	L
					1260	18	Py + L
68	40.0	19.2	34.8 (0.72 at 1293°)**	6.0	1286	4	L
					1275	18	Sil + L
56	40.0	15.0	39.0	6.0	1349	23	L
					1305	17	Sil + L
					1208	47	Sil + L
71	40.0	18.6	32.4	9.0	1249	2	L
					1244	16	Sil + Py + L
67	40.0	19.8	30.0	10.2	1256	2	L
					1245	4	Py + L
66	40.0	18.0	31.8	10.2	1226	12	L
					1224	23	Py + Sil + Mag (tr) + L
					1209	2	Py + Sil + Mag + L
72	40.0	16.8	31.8	11.4	1244	2	L
					1237	10	Sil (tr) + L
54	40.0	21.0	27.0 (0.48 at 1265°)	12.0	1247	3	L
					1238	2	Py + L
					1207	16	Py + Mag + L
					1228	21	Sil + L
					1220	38	Sil + Py + L
					1177	46	Sil + Py + Mag + An + L (SA)

100	45.0	16.5	30.2	8.2	1214	15	L
					1205	2	Py + L
104	45.0	11.0	33.0	11.0	1254	15	L
					1249	4	Sil (tr) + L
101	45.0	16.5	27.5	11.0	1229	23	L
					1228	22	Mag + L
					1175	28	Mag + Py + ? + L (SA)
102	45.0	19.2	24.8	11.0	1247	11	L
					1239	18	Mag + L
					1221	2	Mag + Py + L
131	46.0	14.6	31.9	7.6	1220	22	L
					1214	23	Sil (tr) + L
					1200	3	Sil + An + L
125	46.0	16.2	29.7	8.1	1198	3	L
					1195	14	An + Py + L
					1189	12	An + Py + Mag + Sil + L
					1174	8	An + Py + Sil + ? + L (SA)
150	46.0	14.6	30.8	8.6	1217	16	L
					1205	41	An + L
					1195	24	An + Mag + Sil + L
					1185	12	An + Mag + Sil + Py + L
					1168	7	Crystalline phases + L (SA)
					1159	18	No visible liquid
151	46.0	15.1	29.7	9.2	1214	22	L
					1208	16	An + Mag (tr) + L
					1186	20	An + Mag + Py + Sil + L
					1175	16	Crystalline phases + L (SA)
132	46.0	13.5	30.8	9.7	1217	40	L
			(0.41 at 1245°)		1211	3	Sil (tr) + L
133	46.0	15.7	28.1	10.3	1224	3	L
					1211	3	Mag + L
128	46.0	22.7	18.9	12.4	1279	30	L
					1276	43	Mag (tr) + L
					1224	18	Mag + Py + L
148	46.0	8.1	32.4	13.5	1279	15	L
					1254	6	Hem + L
147	46.0	5.4	32.4	16.2	1287	23	Hem + L
146	46.0	2.7	32.4	18.9	1297	4	Hem + L

TABLE 3 (Continued)

Preparation no.	Composition (wt %) $CaAl_2Si_2O_8$	Mg_2SiO_4	SiO_2	Fe as Fe_3O_4	Temp (°C)	Time (hr)	Phases present*
126	47.0	15.9	29.2	8.0	1215	7	L
					1211	39	An + L
					1200	2	An + Py + L
129	47.0	22.3	18.6	12.2	1285	17	L
					1274	47	Mag + L
					1223	18	Mag + Py + L
144	48.0	14.0	30.7	7.3	1228	20	L
					1219	12	An (tr) + L
127	48.0	15.6	28.6	7.8	1224	20	L
					1219	4	An (tr) + L
143	48.0	24.4	18.2 (0.31 at 1265°)	9.4	1254	15	L
					1250	22	Py + Mag + L
145	48.0	13.0	29.6	9.4	1241	17	L
					1229	32	An + L
137	48.0	22.9	19.2	9.9	1259	42	L
					1251	4	Mag (tr) + L
130	48.0	21.8	18.2	12.0	1284	22	L
					1277	26	Mag + L
					1219	22	Mag + An + Py + L
138	49.0	22.4	18.9	9.7	1258	16	L
					1247	6	Mag + L
85	50.0	17.5	32.5	0.0	1232	2	Py (tr) + L
					1220	2	Py + An + L
					1213	40	All Crystalline
65	40.0	15.0	33.0 (0.35 at 1274°) (0.36 at 1265°)	12.0	1261	17	L
					1251	2	Sil (tr) + L
63	40.0	19.2	28.2	12.6	1248	4	L
					1242	2	Mag (tr) + L
64	40.0	16.8	30.0	13.2	1265	1	L
					1253	12	Mag (tr) + L

62	40.0	25.2	21.0	13.8	1283	18	L
					1280	15	Mag + L
					1270	19	Mag + Py + L
58	40.0	27.0	18.6	14.4	1305	11	L
					1296	3	Ol (tr) + L
					1252	3	Ol + Mag + L
60	40.0	17.4	28.2	14.4	1275	17	L
			(0.35 at 1284°)		1260	5	Mag (tr) + L
					1199	3	Mag + Py + L
53	40.0	30.0	15.0	15.0	1343	20	L
					1331	6	Mag + L
					1324	3	Mag + Ol + L
61	40.0	25.2	19.8	15.0	1300	2	L
			(0.31 at 1310°)		1287	23	Mag + L
52	40.0	24.0	21.0	15.0	1228	4	L
					1280	44	Mag (tr) + L
					1250	4	Mag + Py + L
55	40.0	15.0	27.0	18.0	1287	2	L
			(0.33 at 1294°)		1274	2	Mag + L
69	40.0	6.0	33.0	21.0	1324	42	L
			(0.54 at 1346°)		1316	45	Mag + Hem + L
					1238	45	Mag + Hem + Sil + L
103	45.0	13.8	35.8	5.5	1259	45	Sil + L
105	45.0	16.5	33.0	5.5	1234	60	L
142	50.0	22.5	22.5	5.0	1244	17	L
			(0.53 at 1264°)		1240	7	Py + L
81	50.0	19.5	24.0	6.5	1238	2	L
					1234	60	An + L
80	50.0	14.5	29.0	6.5	1239	2	L
					1230	2	An + L
					1185	12	An + Mag + Sil + Py + L
					1174	8	An + Mag + Sil + Py + L (SA)
140	50.0	25.0	17.5	7.5	1259	45	L
					1240	8	Py + An + L
141	50.0	22.5	20.0	7.5	1240	13	L
					1234	60	An + Py + L

TABLE 3 (Continued)

Preparation no.	Composition (wt %) $CaAl_2Si_2O_8$	Mg_2SiO_4	SiO_2	Fe as Fe_3O_4	Temp (°C)	Time (hr)	Phases present*
86	50.0	15.0	27.5	7.5	1240	2	L
					1229	13	An + L
154	50.0	26.0	16.0	8.0	1272	16	L
					1254	16	Ol + An + Mag + L
152	50.0	23.0	19.0	8.0	1258	20	L
					1246	5	Py + L
83	50.0	15.5	26.5	8.0	1248	15	L
					1234	24	An + L
153	50.0	24.5	16.5	9.0	1260	40	Mag + L
					1248	16	Mag + Ol + L
139	50.0	22.0	18.5	9.5	1260	4	L
					1245	23	Mag + L
					1243	19	Mag + An + L
84	50.0	17.5	22.5	10.0	1250	16	L
					1241	18	An + L
					1232	11	An + Mag + L
87	50.0	15.5	25.0	10.0	1249	2	L
					1237	2	An + L
					1200	2	An + Py + Mag + L
82	50.0	14.5	24.0	11.5	1253	16	L
					1244	60	An + Mag (tr) + L

* Abbreviations used in this table and not explained previously have the following meanings: Py = pyroxene; Ol = olivine; (SA) = Small Amount.

** See corresponding footnote for table 2.

TABLE 4

Results of quenching experiments at an oxygen partial pressure of 10^{-7} atm for the system Mg_2SiO_4-FeO-Fe_2O_3-$CaAl_2Si_2O_8$-SiO_2

Preparation no.	Composition (wt %) $CaAl_2Si_2O_8$	Mg_2SiO_4	SiO_2	Fe as Fe_3O_4	Temp (°C)	Time (hr)	Phases present*
169	35.0	3.3	26.0	35.7	1205	24	Mag + L
176	35.0	6.5	19.5	39.0	1203	48	Mag + L
172	35.0	8.5	24.7	31.8	1224	22	Mag + L
					1181	17	Mag + L
168	35.0	9.8	29.2	26.0	1232	15	Mag + L
					1203	48	Mag + L
					1181	17	Mag + Sil + L
179	35.0	13.7	33.8	17.5	1224	22	L
					1204	17	Mag + Py + L
173	35.0	16.3	26.0 (2.97 at 1180°)** (2.69 at 1178°)	22.7	1232	15	Mag + L
					1201	18	Mag + Py + L
174	35.0	19.5	29.3	16.2	1201	18	Py + L
178	35.0	22.8	32.5	9.7	1231	24	Py + L
163	40.0	3.0	27.0	30.0	1224	22	Mag + An + L
69	40.0	6.0	33.0	21.0	1223	24	L
					1217	26	Mag + L
164	40.0	9.0	21.0	30.0	1236	22	Mag + L
					1224	24	Mag + An (tr) + L
162	40.0	9.0	27.0	24.0	1213	24	Mag + L
64	40.0	16.8	30.0	13.2	1247	23	L
					1223	24	Py + L

TABLE 4 (Continued)

Preparation no.	Composition (wt %)				Temp (°C)	Time (hr)	Phases present*
	$CaAl_2Si_2O_8$	Mg_2SiO_4	SiO_2	Fe as Fe_3O_4			
60	40.0	17.4	28.2	14.4	1247	23	L
					1224	21	Py + L
166	40.0	18.0	18.0	24.0	1250	23	Mag + L
					1212	22	Mag + Ol + L
66	40.0	18.0	31.8	10.2	1223	24	Py + L
					1139	10	Completely crystalline
63	40.0	19.2	28.2	12.6	1224	22	Py + L
52	40.0	24.0	21.0	15.0	1250	23	Ol + L
61	40.0	25.2	19.8	15.0	1238	26	Ol + L
53	40.0	30.0	15.0	15.0	1250	23	Ol + L
104	45.0	11.0	33.0	11.0	1205	21	An + L
101	45.0	16.5	27.5	11.0	1224	22	L
					1205	24	Py + An + L
146	46.0	2.7	32.4	18.9	1238	26	Mag + An + Sil + L
148	46.0	8.1	32.4	13.5	1223	24	An (tr) + L
149	46.0	10.8	29.7	13.5	1224	21	An (tr) + L
132	46.0	13.5	30.8	9.7	1205	21	An + L
131	46.0	14.6	31.9	7.6	1224	24	L
					1205	24	An + L
133	46.0	15.7	28.1	10.3	1224	21	L
					1205	24	Py + An + L
128	46.0	22.7	18.9	12.4	1238	26	Ol + L
					1224	24	Ol + Py + An + L

* See footnotes of previous tables for explanation of abbreviations.
** See corresponding footnote for table 2.

TABLE 5

Results of quenching experiments at an oxygen partial pressure of 10^{-9} atm for the system Mg_2SiO_4-FeO-Fe_2O_3-$CaAl_2Si_2O_8$-SiO_2

Preparation no.	Composition (wt %)				Temp (°C)	Time (hr)	Phases present*
	$CaAl_2Si_2O_8$	Mg_2SiO_4	SiO_2	Fe as Fe_3O_4			
169	35.0	3.2	26.0	35.8	1201	23	L
					1178	23	Mag + Sil + An (tr) + L
172	35.0	8.5	24.7 (3.62 at 1180°)**	31.8	1199	24	L
168	35.0	9.8	29.2 (3.20 at 1176°)	26.0	1179	23	L
					1153	24	Mag + Py + Sil + L
179	35.0	13.7	33.8	17.5	1178	23	Py + L
173	35.0	16.3	26.0	22.7	1178	23	Py + L
					1152	24	Py + Mag + L
200	36.4	12.6	20.2	30.8	1178	23	Mag + L
					1162	24	Mag + Py + An + L
199	37.2	17.9	23.0	21.9	1178	23	Ol + Py + L
163	40.0	3.0	27.0	30.0	1201	22	L
					1179	22	Mag + An + Sil + L
167	40.0	6.0	18.0	36.0	1199	24	Mag + An (tr) + L
69	40.0	6.0	33.0	21.0	1180	23	Sil (tr) + L
164	40.0	9.0	21.0	30.0	1201	23	L
					1179	22	Mag (tr) + An (tr) + L

TABLE 5 (Continued)

Preparation no.	Composition (wt %) $CaAl_2Si_2O_8$	Mg_2SiO_4	SiO_2	Fe as Fe_3O_4	Temp (°C)	Time (hr)	Phases present*
162	40.0	9.0	27.0	24.0	1178	18	L
					1165	21	Mag + An + L
					1152	20	Mag + An + Sil + Py + L
185	40.0	11.4	32.4	16.2	1180	24	Sil + L
183	40.0	13.8	22.2 (3.66 at 1172°)	24.0	1179	22	L
					1165	21	Py + An + L
182	40.0	15.0	15.0	30.0	1201	22	Ol + Mag + L
	40.0	15.0	27.0	18.0	1180	24	Py + L
166	40.0	18.0	18.0	24.0	1181	23	L
					1165	21	An + Ol + L
					1152	20	An + Py + L
186	40.0	19.2	24.6	16.2	1199	23	Py + L
184	40.0	19.8	21.0	19.2	1201	22	Ol + Py + L
					1180	24	Ol + Py + An + L
188	40.0	24.0	15.0	21.0	1199	24	An + Ol + L
	41.8	32.1	57.0	10.7	1202	18	Py + L
167	44.7	6.7	20.1	28.5	1171	20	Mag + An + L

* See footnotes of previous tables for explanation of abbreviations.
** See corresponding footnote for table 2.

TABLE 6

Results of quenching experiments at an oxygen partial pressure of 10^{-11} atm for the system Mg_2SiO_4-FeO-Fe_2O_3-$CaAl_2Si_2O_8$-SiO_2

Preparation no.	Composition (wt %)				Temp (°C)	Time (hr)	Phases present*
	$CaAl_2Si_2O_8$	Mg_2SiO_4	SiO_2	Fe as Fe_3O_4			
171x	30.0	10.5	28.0	31.5	1130	24	Ol + Py + L
					1110	22	Ol + Py + L
202x	30.2	2.8	22.4 (4.33 at 1134°)**	44.6	1131	24	L
204x	31.2	8.7	26.1 (4.39 at 1156°)	34.1	1133	22	Ol + Py + L
201x	31.2	14.5	23.2	31.0	1131	24	Ol + Py + L
203x	31.4	5.8	17.5	45.3	1131	24	Ol + Mag + L
34	34.0	0.0	36.0 (4.26 at 1146°)	30.0	1130	23	Sil + L
169x	35.0	3.3	26.0 (4.38 at 1134°)	35.7	1131	24	L
					1110	22	An + L
176x	35.0	6.5	19.5 (4.45 at 1152°)	39.0	1129	22	An + L
172x	35.0	8.5	24.7 (4.27 at 1133°)	31.8	1131	24	L
					1110	22	Ol + An + L
168x	35.0	9.8	29.2	26.0	1129	22	Py + L
179x	35.0	13.7	33.8	17.5	1130	23	Sil + Py + L
173x	35.0	16.3	26.0	22.7	1150	42	Ol + Py + L
174x	35.0	19.5	29.3	16.2	1130	23	Py + L
195x	35.3	5.3	15.9	43.5	1132	23	Mag + An + L

TABLE 6 (Continued)

Preparation no.	Composition (wt %) $CaAl_2Si_2O_8$	Mg_2SiO_4	SiO_2	Fe as Fe_3O_4	Temp (°C)	Time (hr)	Phases present*
197x	35.7	8.0	24.2 (4.57 at 1130°)	32.0	1131	22	L
200x	36.4	12.6	20.2	30.8	1133	22	Ol + L
168	37.2	10.4	31.1	21.5	1149	23	Py + L
169	37.4	3.5	27.8	31.3	1149	23	An + Sil + L
196	37.5	16.9	16.9	28.8	1179	24	Ol + Mag + L
197	38.0	8.5	25.7	27.9	1151	23	L
172	38.5	9.2	27.2	25.1	1150	23	L
197	39.0	8.7	26.4	25.9	1149	23	An + L
196	39.1	17.6	17.6	25.7	1178	23	Ol + Mag + L
179	39.4	15.3	38.2	7.1	1210	23	Sil + L
198	39.9	11.4	32.3	16.5	1147	23	Py + L
163x	40.0	3.0	27.0	30.0	1132	24	An + Sil + L
167x	40.0	6.0	18.0	36.0	1130	23	An + Mag (tr) + L
164x	40.0	9.0	21.0	30.0	1149	20	An + L
200	40.0	13.9	22.2	23.9	1153	45	Ol + Py + An + L
73	40.4	33.3	24.8	1.4	1252	25	Py + L
186	40.7	19.6	25.1	14.7	1180	24	Py + L
195	40.9	6.1	18.4	34.6	1147	23	An + Mag + L
173	40.9	19.0	30.4	9.7	1180	51	Py + L
68	40.9	19.6	35.6	3.9	1250	22	Py + Sil + L
65	41.2	15.5	34.0	9.1	1181	23	Py + Sil (tr) + L
51	41.2	21.6	34.0	3.2	1251	23	Py + L
53	41.6	31.2	15.5	11.7	1210	24	Ol + An + L

71	41.8	19.4	33.8	5.1	1210	23	Py + L
50	41.8	31.3	25.1	1.8	1250	24	Py + L
64	41.9	17.6	31.5	9.0	1181	23	Py + L
162	42.0	9.4	28.3	20.2	1180	45	An (tr) + L
183	42.1	14.6	23.4	20.1	1180	24	Ol + An + L
200	42.3	14.6	23.4	19.7	1180	23	Ol + An (tr) + L
54	42.6	22.4	28.8	6.2	1209	24	Py + L
72	43.4	18.2	34.4	4.1	1181	23	Py + L
185	43.7	12.5	35.4	8.5	1210	23	Sil + L
163	43.9	3.3	29.6	23.4	1196	45	An (tr) + L
166	43.9	19.7	19.7	16.8	1177	23	Ol + Py + An + L
52	43.9	26.3	23.1	6.7	1210	24	Ol +Py + An + L
53	44.1	33.1	16.5	6.3	1251	23	Ol + L
176	44.2	8.2	24.6	23.0	1179	51	An (tr) + L
69	44.6	6.7	36.8	11.9	1210	23	Sil + L
52	44.7	26.8	23.5	4.9	1251	45	Ol + L
55	45.1	16.9	30.4	7.6	1178	45	Py + An + L
58	45.5	30.8	21.2	2.8	1251	23	Ol + Py + L
183	45.7	15.7	25.3	13.3	1211	22	L
188	46.2	27.8	17.3	8.8	1251	23	Ol + L
164	46.4	10.4	24.3	19.0	1179	23	An + L
69	46.7	7.0	38.6	7.7	1179	23	Sil + An (tr) + L
163	46.9	3.5	31.6	18.0	1180	45	An + Sil + L
166	47.5	21.4	21.4	9.7	1251	45	Ol + L
167	49.9	7.5	22.4	20.2	1178	18	An + L
130	49.9	22.7	18.9	8.6	1182	24	Ol + Py + L
149	50.1	11.8	32.4	5.8	1179	29	An + Sil + L
182	51.0	19.1	19.1	10.9	1251	45	Ol (tr) + L

* See footnotes of previous tables for explanation of abbreviations.
** See corresponding footnote for table 2.

TABLE 7

Al_2O_3 in magnetite from mixtures run at an oxygen partial pressure of $10^{-0.7}$ atm (air)

Preparation no.	Composition (wt %)				Temp (°C)	Spinel (311) "d" Spacing	Range* of Al_2O_3 (mole %)
	$CaAl_2Si_2O_8$	Mg_2SiO_4	SiO_2	Fe as Fe_3O_4			
—	—	—	—	100.0	1450	2.531	0
12	30.0	—	—	70.0	1394	2.516	8-13
11	40.0	—	—	60.0	1392	2.515	9-14
3	50.0	—	—	50.0	1410	2.510	11-18
9	60.0	—	—	40.0	1413	2.514	9-15
9	60.0	—	—	40.0	1362	2.516	8-13
4	66.7	—	—	33.3	1386	2.516	8-13
60	40.0	17.4	28.2	14.4	1204	2.525	3-6
53	40.0	30.0	15.0	15.0	1237	2.503	15-22
55	40.0	15.0	27.0	18.0	1243	2.514	9-15
69	40.0	6.0	33.0	21.0	1209	2.517	7-13
69	40.0	6.0	33.0	21.0	1190	2.520	6-10
69	40.0	6.0	33.0	21.0	1175	2.522	5-9

* Range of mole % Al_2O_3 in spinel solid solution was found by plotting (311) "d"-spacing on curves shown in figure 4 and explained in text.

TABLE 8

Al_2O_3 in hematite from mixtures run at oxygen partial pressure of $10^{-0.7}$ atm (air)

Preparation no.	$CaAl_2Si_2O_8$	SiO_2	Fe as Fe_3O_4	Temp (°C)	Hematite (124) "d" spacing	Mole % Al_2O_3*
—	—	—	100.0	1200	1.485_9	0
—	—	—	100.0	Directly from reagent bottle	1.485_7	0
13	20.0	—	80.0	1374	1.482_1	3
13	20.0	—	80.0	1373	1.481_2	5
12	30.0	—	70.0	1332	1.480_8	5
8	70.0	—	30.0	1373	1.479_0	8
7	80.0	—	20.0	1332	1.478_7	8
36	62.0	15.0	23.0	1317	1.481_0	5

* Mole % of Al_2O_3 in hematite was found by plotting (124) "d"-spacing on curve published by Muan and Gee (1956).

TABLE 9

Approximate composition and liquidus temperature of certain points in diagrams

Point	pO_2 (atm)	Composition (wt %)					Temp (°C)	Crystalline phases at liquidus**	Found in following figures
		SiO_2	Fe as Fe_3O_4	MgO	CaO	Al_2O_3			
c	$10^{-0.7}$	40	41	19	0	0	1375 ± 5	Py + Mag + Ol	1, 2, 3, 9, 10
d	$10^{-0.7}$	45	39	16	0	0	1366 ± 5	Py + Mag + Sil	1, 2, 4, 9, 10
s	10^{-9}	34	66	0	0	0	1140 ± 5	Fay + Mag + Sil	1, 5
P or P′	$10^{-0.7}$	49	9	14	10	18	1240 ± 10	An + Py + Ol + Mag	9, 10, 12, 13
E or E′	$10^{-0.7}$	57	8	9	9	17	1185 ± 10	An + Py + Sil + Mag	9, 10, 12, 13, 14
F or F′	10^{-7}	55	14	6	9	16	1155 ± 20	An + Py + Sil + Mag	10, 12, 13, 14
G or G′	10^{-9}	51	21	6	8	14	1120 ± 20	An + Py + Sil + Mag	10, 12, 13, 14
B or B′	*	45	38	0	6	11	1050 ± 20	An + Fay + Sil + Mag	5, 13, 14
H or H′	10^{-11}	48	29	4	7	12	1090 ± 20	An + Py + Ol + Sil	10, 12, 13
J or J′	$10^{-0.7}$	56	12	5	10	17	1240 ± 10	An + Sil + Hem + Mag	9, 10, 12, 13
m (Olivine basalt)		45	15	17	8	15		Variable with pO_2: Ol, or Ol + Mag	8a, 11a

* Probably close to that of H and H′, that is, 10^{-11} atm.

** An abbreviation in this table not explained previously: Fay = fayalite.

TABLE 10

Total iron and FeO in quenched mixtures run under conditions as indicated

Preparation no.	Composition of Mixture (wt %) before heat treatment				After heat treatment			Crucible	Temp (°C) and time (hr)	pO_2 (atm)	Phases**
	$CaAl_2Si_2O_8$	Mg_2SiO_4	SiO_2	Fe as Fe_3O_4	Total Fe_3O_4 by analysis	FeO by analysis	FeO/ Fe_2O_3				
73	40.0	33.0	24.6	2.4	2.5	—	—	Pt	1377°-6	$10^{-0.7}$	L
51	40.0	21.0	33.0	6.0	7.3	—	—	Pt	1284°-48	$10^{-0.7}$	L
66	40.0	18.0	31.8	10.2	10.2	—	—	Pt	1230°-48	$10^{-0.7}$	L
68	40.0	19.2	34.8	6.0	—	2.6	0.72	Pt	1293°-24	$10^{-0.7}$	L
54	40.0	21.0	27.0	12.0	—	4.0	0.48	Pt	1265°-19	$10^{-0.7}$	L
65	40.0	15.0	33.0	12.0	—	3.2	0.35	Pt	1274°-17	$10^{-0.7}$	L
65	40.0	15.0	33.0	12.0	—	3.3	0.36	Pt	1265°-18	$10^{-0.7}$	L
60	40.0	17.4	28.2	14.4	—	3.8	0.35	Pt	1284°-21	$10^{-0.7}$	L
61	40.0	25.2	19.8	15.0	—	3.6	0.31	Pt	1310°-18	$10^{-0.7}$	L
55	40.0	15.0	27.0	18.0	—	4.6	0.33	Pt	1294°-24	$10^{-0.7}$	L
69	40.0	6.0	33.0	21.0	—	7.3	0.54	Pt	1346°-5	$10^{-0.7}$	L
132	46.0	13.5	30.8	9.7	—	2.9	0.41	Pt	1245°-17	$10^{-0.7}$	L
143	48.0	24.4	18.2	9.4	—	2.3	0.31	Pt	1265°-18	$10^{-0.7}$	L
28	48.0	—	42.0	10.0	—	3.1	0.45	Pt	1332°-22	$10^{-0.7}$	L
142	50.0	22.5	22.5	5.0	—	1.8	0.53	Pt	1264°-45	$10^{-0.7}$	L
30	50.0	—	30.0	20.0	—	7.0	0.55	Pt	1335°-18	$10^{-0.7}$	L
25	52.0	—	38.0	10.0	—	3.4	0.52	Pt	1314°-26	$10^{-0.7}$	L
169	35.0	3.3	26.0	35.7	31.8	—	—	Pt	1205°-24	10^{-7}	Mag + L
163	40.0	3.0	27.0	30.0	30.8	—	—	Pt	1224°-22	10^{-7}	Mag + An + L

TABLE 10 (Continued)

Preparation no.	Composition of mixture (wt %) before heat treatment				After heat treatment			Crucible	Temp (°C) and time (hr)	pO_2 (atm)	Phases**
	$CaAl_2Si_2O_8$	Mg_2SiO_4	SiO_2	Fe as Fe_3O_4	Total Fe_3O_4 by analysis	FeO by analysis	FeO/Fe_2O_3				
164	40.0	9.0	21.0	30.0	31.6	—	—	60Ag40Pd	1213°-24	10^{-7}	Mag + An + L
164	40.0	9.0	21.0	30.0	29.8	—	—	Pt	1224°-24	10^{-7}	Mag + An (tr) + L
166	40.0	18.0	18.0	24.0	24.5	—	—	Pt	1250°-23	10^{-7}	Mag + L
131	46.0	14.6	31.9	7.6	8.6	—	—	Pt	1205°-24	10^{-7}	An + L
173	35.0	16.2	26.0	22.8	—	16.3	2.97	60Ag40Pd	1180°-50	10^{-7}	Mag + Py + L
173	35.0	16.2	26.0	22.8	—	15.9	2.69	60Ag40Pd	1178°-45	10^{-7}	Mag + Py + L
168	35.0	9.8	29.2	26.0	24.6	17.8*	3.20	55Ag45Pd	1176°-21	10^{-9}	L
172	35.0	8.4	24.7	31.8	30.0	22.3*	3.62	55Ag45Pd	1180°-29	10^{-9}	L
183	40.0	13.8	22.2	24.0	21.6	16.1*	3.66	55Ag45Pd	1172°-24	10^{-9}	Py + An + L
172	35.0	8.4	24.7	31.8	31.0	—	—	60Ag40Pd	1130°-24	10^{-11}	L
169	35.0	3.2	26.0	35.8	37.4	—	—	60Ag40Pd	1130°-24	10^{-11}	L
164	40.0	9.0	21.0	30.0	29.4	—	—	60Ag40Pd	1130°-24	10^{-11}	An + Ol + L
202	30.2	2.8	22.4	44.6	38.7	29.8*	4.33	55Ag45Pd	1134°-15	10^{-11}	L
204	31.2	8.7	26.1	34.1	27.3	21.1*	4.39	55Ag45Pd	1156°-23	10^{-11}	DND
34	34.0	—	36.0	30.0	23.8	18.3*	4.26	55Ag45Pd	1146°-22	10^{-11}	Sil + L
172	35.0	8.4	24.7	31.8	29.5	22.7*	4.27	55Ag45Pd	1133°-16	10^{-11}	Ol + An + L
169	35.0	3.2	26.0	35.8	33.1	25.5*	4.38	55Ag45Pd	1134°-24	10^{-11}	An + L
176	35.0	6.5	19.5	39.0	32.4	25.1*	4.45	55Ag45Pd	1152°-24	10^{-11}	An + Ol (tr) + L
197	35.7	8.0	24.2	32.0	27.7	21.6*	4.57	55Ag45Pd	1130°-16	10^{-11}	L

* Analysis performed by C. O. Ingamells.

** Abbreviations used in this table and not explained previously have the following meanings: DND = Did Not Determine.